Evolution of atomically precise clusters through the eye of mass spectrometry

Shridevi Bhat, Indranath Chakraborty, Ananya Baksi, Raghu Pradeep Narayanan and Thalappil Pradeep*

DOI: 10.1039/9781782623717-00343

Enormous developments in the area of soluble noble metal clusters protected with monolayers are discussed. Mass spectrometry has been the principal tool with which cluster growth has been examined. The composition and chemistry of clusters have been examined extensively by mass spectrometry. Besides gold, silver, platinum, copper and iron clusters have been examined. Clusters have also been examined by tandem mass spectrometry and the importance of ligands in understanding closed shell electronic structure is understood from such studies. Protein protected noble metal clusters belong to a new group in this family of materials. Naked metal clusters bearing the same core composition as that of monolayer protected clusters is another class in this area, which have been discovered by laser desorption ionization from protein templates.

1 Introduction

Mass spectrometry, just after a century of its existence continues to be one of the most important workhorses of chemistry.[1,2] Over the years, it has become the single most important analytical tool in proteomics, metabolomics and several other disciplines.[3,4] Traditional materials science has been away from the influence of mass spectrometry as tools of solid state materials science such as X-ray diffraction, electron microscopy, electron spectroscopy and several others continue to be the principal means of analysis of solids.[1–39] However, when dimension of matter reduces to the ultra-small regime, of the order of a nanometer, materials science requires mass spectrometry for detailed characterisation. This chapter explores this emerging influence of mass spectrometry in materials science taking noble metal clusters (M_n) as examples.

There are two important aspects of mass spectrometry relevant in the context of M_n clusters. Mass analysis involves ionization which invariably imparts internal energy to the species. There is a need to reduce the energy input into the clusters as they are susceptible to rapid fragmentation as clusters in general are metastable, in comparison to the bulk. In a cluster system, there could be several closely lying minima and interconversion between them may become feasible due to the acquired internal energy. As a result, to study a cluster in its native form, it is required to minimize the internal energy input during ionization.

This requirement necessitates adaptation of soft ionization methods for ionizing clusters. The common methods of ionization are

DST Unit of Nanoscience (DST UNS) and Thematic Unit of Excellence, Department of Chemistry, Indian Institute of Technology Madras, Chennai 600 036, India. E-mail: pradeep@iitm.ac.in

Electrospray Ionization (ESI) and Matrix Assisted laser Desorption Ionization (MALDI).[8,9,22,28,40–47] Both have been employed successfully in a number of cases. However, as neither of them gives complete information, often a combination of the two is necessary for definite finger printing. Clusters are protected entities and charge incorporation into the system during ionization is often due to the ligand. In the case of functionalized ligands such as carboxyl (-COOH), amine (-NH_2), *etc*., a loss or acquisition of proton is the principal means of ionization. Therefore, pH control of the solution becomes an easy method in ESI. In several others, charge is brought into the system through metal incorporation as in case of Cs^+ adducts.[31] Mechanism of ionization in MALDI is still unclear in this system. As a result, exploration of various matrices and ionization conditions becomes necessary to observe reliable ionization of the cluster systems.

Ionization does not always lead to accurate mass analysis. As the clusters are fragile, fast analysis is necessary to reduce metastable decay. Mass spectrometers with adequate mass range and improved stability in such mass ranges are required as analysis often involves long time acquisition of data. Understanding of isotope distribution as a whole is needed which requires improved mass resolution at this mass range.[22,42] Therefore, the most successful analysis involves TOF or Q-TOF.

Identification of the parent ion is confirmed in a few cases by MS/MS analysis.[15] In a cluster system, this requires increased ion intensity as well as improved mass range of analysis. As most instruments and most cluster systems do not simultaneously meet the requirements, such analyses are done only in few cases. Improved understanding of such clusters is feasible by the use of multiple methodologies.

As can be seen from the preceding paragraphs, mass spectrometry along with separation techniques have helped in the identification of new cluster systems.[48] In many cases, it has been mass spectrometry that has contributed to cluster science than crystallography. However, increasing capability, both in resolution and mass range as well as better ionization methods, would be necessary to grow the subject area further. While the current contribution of mass spectrometry is often limited to identification, more efforts are needed in exploring the properties of clusters by mass spectrometry, which requires better MS/MS capabilities. Clusters, because of their different conformations and due to the existence of isomers there is a need to undertake other analyses along with mass spectrometry. This is now possible with commercial instruments by Ion Mobility Mass Spectrometry (IMS). New efforts in this direction are happening in the past few years.

2 Clusters of the past

Cluster may be defined as a constitution of bound atoms or molecules which exhibit completely different properties than the corresponding bulk materials.[49–51] Their properties vary drastically with size. There have been numerous developments in the area of clusters existing in gaseous and condensed phases.

2.1 Gas phase clusters

Gas phase clusters are extremely reactive and as a result they cannot be stored in ambient conditions.[52] Always such clusters are made *in situ* where experimental properties are studied. Several techniques have been implemented to make such clusters in the gas phase; examples are the evaporation of metals by heating and ion/laser bombardment, *etc*. Laser vaporization techniques in conjunction with mass spectrometry have been used widely to investigate clusters precisely. Based on the constitution and properties, gas phase clusters have been classified as ionic, covalent, metal, semiconductor, molecular, *etc*. We will discuss a few of them.[52]

2.1.1 Metal clusters. Metal clusters are made of different metals like alkali, alkaline earth and transition metals.[51] Plenty of reports are there especially on sodium clusters.[37,53,54] Such clusters are produced in a gas aggregation source where the metals (such as sodium) are heated at $\sim 400\,^{\circ}C$. The hot vapor is then passed through a low vacuum He-atmosphere ($T = 77$ K) to produce clusters of different sizes. Quadrupole mass analysers (QMA) are used to identify the clusters. Clusters up to 150 atoms have been observed. Knight *et al*. have observed a discontinuous variation in intensity at $N = 2$, 8, 20, 40, 58, and 92 (magic numbers) in the mass spectra of Na clusters.[53] Explanation for this pattern of intensity has been made based on the one-electron shell model in which 3s valence electrons are bound in a spherically symmetric potential well. These correspond to closed electronic shells. Similarly Katakuse *et al.* have shown the different ion intensities in the mass spectra of silver clusters (Ag_x).[23] In this case, silver clusters with an odd number of atoms are more intense compared to those with an even number which again can be explained by simply counting the number of valence electrons. The clusters with odd number of atoms have even number of valence electrons which results in spin pairing and that enhances the stability compared to those with even number of atoms.[30] It is also noticeable that just after these peaks, there is a sharp decrease in the intensity of the next peak. Guo *et al*. have demonstrated the direct generation of large silver cluster ions through laser desorption ionization of silver-containing salts without the assistance of a molecular beam.[55] Both positively and negatively charged silver clusters up to $N = 100$ have been produced using this method. The distributions are similar to those produced using the beam-based approaches. Here also two special features have been observed; first, the cluster intensity distribution displays an odd–even alternation pattern and the second, a steep decrease of ion intensities after some clusters called 'magic numbers'. Au and Cu have also been studied extensively[23,24] and lots of recent reports also exist to utilize them in cluster catalysis.[7]

2.1.2 Semiconductor clusters. Semiconductor clusters are mainly generated from the semiconducting elements such as silicon,[57,59–62] carbon[63,64] and germanium.[65] After the great discovery of the fullerene (mass spectrum of C_{60} is given in Fig. 1A),[56] researchers have shown

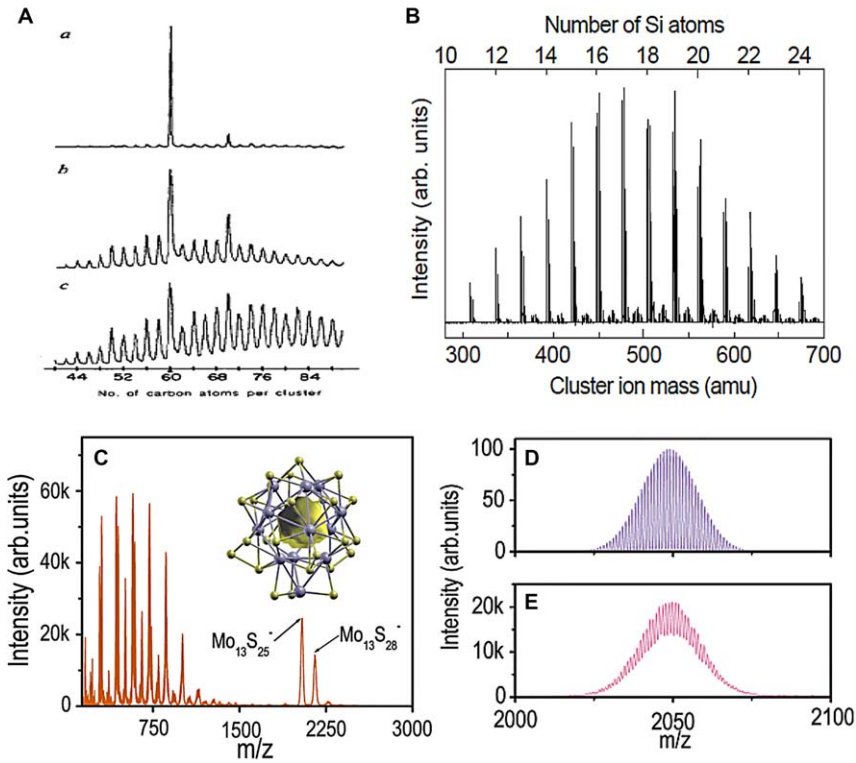

Fig. 1 (A) TOF mass spectra of carbon clusters prepared by laser vaporisation of graphite and cooled in a supersonic beam. The extent of He collision occurring in the supersonic nozzle (decreases from a to c). Reproduced with permission.[56] ©Nature publishing. (B) Mass spectrum of silicon clusters. Reproduced with permission.[57] © Heat Transfer Society of Japan. (C) Negative mode LDI mass spectrum of MoS_2 nanoflakes. Inset shows the structure of the $Mo_{13}S_{25}$ cluster. The expanded mass spectrum of $Mo_{13}S_{25}$ cluster (D) is plotted along with the calculated one (E), which shows an exact match. ©ACS publishing. Reproduced with permission.[58]

enormous interest to explore the possibility of other semiconductor clusters. As the bonding between carbons is covalent in nature, they have the tendency to form a variety of clusters compared to other elements. Several series of carbon clusters including C_{60}, C_{70}, *etc*. are reported now.[56] Other than carbon, various kinds of gas phase Si clusters are known and Maruyama *et al*.[57] have shown a series of clusters starting from $N = 8$ to 24 produced by pulsed laser-vaporization supersonic-expansion cluster beam source, directly connected to a FT-ICR spectrometer (Fig. 1B). Then the injected and size selected silicon clusters were cooled to room temperature by collision with argon.

2.1.3 Molecular clusters. Several kinds of gas phase molecular clusters exist in the literature.[27,33,58,66–70] Inorganic molecular structures such as polyoxymolybdates are examples of such kind.[71] Usually, they form cage like structures which are often called inorganic fullerenes (IFs).[72–75] IFs were originally made from the layered structured chalcogenide MX_2 where M = Mo, W and X = S, Se.[72,76–85] Different

methodologies have been applied to make IFs in the gas phase. To fold such layered structure to form cages or closed cylinders, high energy is needed which is supplied by arc discharge, laser vaporisation, ultrasonication or other sources.[56,86,87] Singh *et al*. have synthesized such a novel cage cluster of MoS_2 in the gas phase by laser evaporation.[58] Bulk MoS_2 was ground well and dispersed in acetone which was spotted on a MALDI plate and a pulsed laser of 337 nm was applied to get the clusters. The mass spectrum has been collected in the negative mode. LDI MS data shows a series of clusters such as MoS_2^-, MoS_3^-, MoS_4^-, $Mo_2S_3^-$, $Mo_2S_5^-$, $Mo_2S_6^-$, $Mo_2S_8^-$, and so on. The spectrum exhibits a trend of increase in intensity starting from MoS_2^- and it reaches a maximum around $Mo_4S_7^-$, and decreases thereafter. After this region (Fig. 1C), the spectrum is completely featureless till *m*/*z* 2000, and suddenly, an intense peak appears at *m*/*z* 2049, which was followed by another peak at *m*/*z* 2144. An expanded view of the peak at *m*/*z* 2049 is shown in Fig. 1D which shows an exact match with the corresponding calculated spectrum of $Mo_{13}S_{25}$ (Fig. 1E). Similarly the next peak was assigned as $Mo_{13}S_{28}^-$. Along with this type of molybdenum sulfide cluster, several other clusters such as WS_2, layered metal halides such as $NiCl_2$, $CdCl_2$, and $TlCl_3$ and oxides such as TiO_2 and V_2O_5 also produced gas phase molecular clusters.[88] Gas phase clusters of noble metals have also been studied and clusters such as Au_n,[23] Ag_n,[23,55] *etc*. have been detected.

2.2 Early stages of monolayer protected clusters

Along with gas phase transition metal clusters, mass spectrometry has given an useful method to analyze noble metal cluster systems.[19] These clusters are monolayer protected by means of a ligand and as a result, they can be synthesized in solutions. Just after the Brust's new synthetic protocol,[89] scientists have started synthesizing highly monodisperse nanoparticles which show molecule – like optical features. Researchers from different groups have realised the importance of mass spectrometry in studying such clusters.[9,10,12,22,25,26,40–42,44,90–97] Initially, LDI was used to identify the core mass.[91,93] A variety of clusters having different core masses have been identified in those decades. In most of the cases, clusters are protected with alkane thiols.[91,93] Whetten *et al.* have shown a series of clusters starting from 27 kDa to 93 kDa (Fig. 3A).[98] Based on the TEM analysis and mass spectral position, it has been suggested that the core contains 140 to 459 gold atoms. Reports of glutathione protected clusters are also there. Initially, the 5.6 kDa cluster (core mass) detected by LDI mass spectrometry was assigned as $Au_{28}(SG)_{18}$.[99] Then in 2005, Negishi *et al*. have reassigned the cluster as $Au_{25}(SG)_{18}$ based on high resolution electrospray analysis.[47] The clusters have been synthesized by reducing the Au(I)-SG polymer in ice cold condition which produces a mixture of clusters. In a later report, they have isolated nine clusters (1–9) through polyacrylamide gel electrophoresis (PAGE). These isolated cluster samples have been measured by their home – built ESI apparatus.[47] A schematic of the instrument is given in Fig. 2A which consists of five stages of differentially pumped vacuum chambers. The apparatus

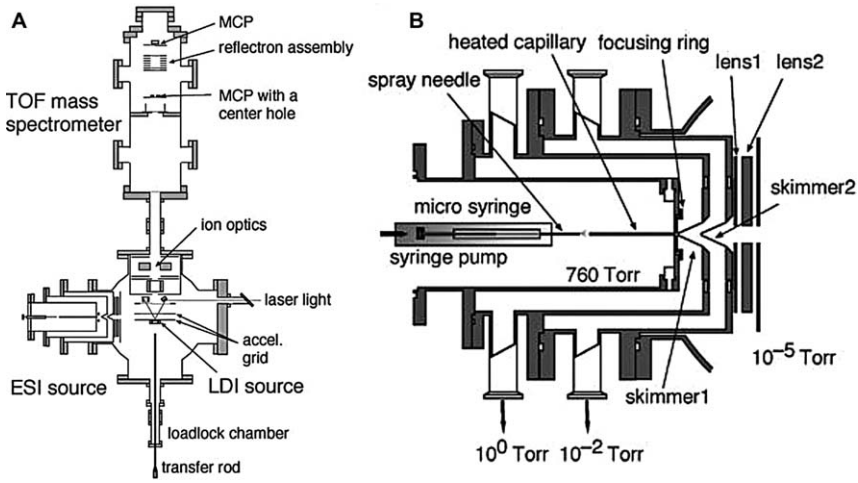

Fig. 2 (A) Schematic view of the TOF mass spectrometer equipped with electrospray ionization (ESI) and laser desorption ionization (LDI) sources. (B)The details of the ESI source. ©ACS Publishing. Reproduced with permission.[47]

accommodates an ESI source for the production of gaseous ions of metal clusters dispersed in a solvent and a time-of-flight (TOF) mass spectrometer with a reflectron. Schematic of the ESI source is given in Fig. 2B, along with the typical pressures of the chambers under operation. For a typical measurement, 50% (v/v) water/methanol solutions of the Au : SG clusters with a concentration of 0.5 mg mL^{-1} were electrosprayed into the ambient atmosphere through a syringe (flow rate of 2 μL min^{-1}) biased at *ca.* −3 kV. The central part of the sprayed cone containing large droplets was fed into a capillary heated resistively to promote desolvation. Capillary temperature was optimized so that evaporation of the solvents from the droplets proceeds efficiently which results in maximum intensity of the desolvated cluster ions in the intact form. At higher capillary temperature, small fragments such as $[Au(SG)_2\text{-}H]^{-1}$ and $[Au_2(SG)_2\text{-}H]^{-1}$ have been observed.[47] The cluster ions exiting the capillary were focused by a ring electrode, skimmed by two sets of skimmers, and guided by an einzel lens towards an acceleration region of the TOF mass spectrometer of a Wiley-McLaren-type configuration. The ions were extracted perpendicularly to the initial beam by applying a pulsed high voltage (*ca.* −9 to −14 kV with ∼30 ns rise time and 100 μs duration) to the acceleration grids. After stirring and focusing by sets of ion optics, the ions were counted either by a microchannel plate detector located at the end of the flight path (F4655-10, Hamamatsu) or by that with a centre hole (LPD-25, Burle) after reflecting back by the retarding field of the reflectron. The repetition rate was 130 Hz, and spectra were obtained by accumulation for 5–40 min. Resolutions of the mass spectrometer (M/ΔM) with and without the reflectron were typically 1000 and 400, respectively. All the clusters have been identified based on their peak positions and isotopic distributions. The clusters (1–9) have been assigned as $Au_{10}(SG)_{10}$, $Au_{15}(SG)_{13}$, $Au_{18}(SG)_{14}$, $Au_{22}(SG)_{16}$, $Au_{22}(SG)_{17}$, $Au_{25}(SG)_{18}$, $Au_{29}(SG)_{20}$, $Au_{33}(SG)_{22}$, and $Au_{39}(SG)_{24}$, respectively (Fig. 3B). This was the very first

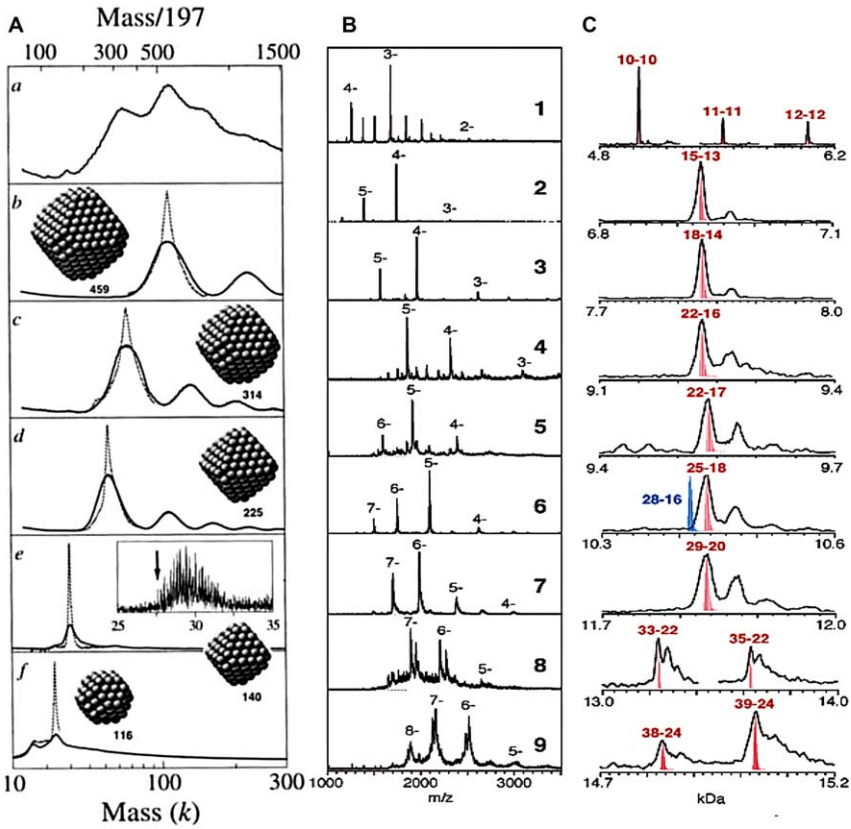

Fig. 3 (A) Mass spectra of the crude mixture (a) and of isolated fractions (b–e) of dodecane thiol protected gold clusters. Inset shows the structures predicted from optimal cores of $N = 459$, 314, *etc.* gold atoms. ©Wiley-VCH publishing. Reproduced with permission.[98] (B) Low resolution ESI mass spectra of the isolated clusters (1–9). (C) The high resolution spectra of the same. The trace shows the corresponding calculated spectra for $Au_n(SG)_m$ clusters with the corresponding n–m values. ©ACS publishing. Reproduced with permission.[47]

report of a complete ESI MS assignment of a series of glutathione protected clusters. Among them, crystal structure of $Au_{25}(SR)_{18}$ have been solved in 2008[100] which emphasized the capability of mass spectrometry in assigning such clusters precisely.

3 Advances in cluster science

Enormous expansion has happened in the field of nanoclusters and researchers have shown an effective role of mass spectrometry in characterizing such pieces of matter. It is important to mention here that mass spectrometry is not the only tool to characterize such clusters. Crystal structure is very much important to understand the detailed structure. Although there are plenty of reports of clusters assigned through mass spectrometry, only a few of them have been crystallized. A brief discussion of the clusters crystallized is given in Table 1. In general, the structures consist of a metallic core which are surrounded by

Table 1 List of clusters with crystal structures.

Numbers	Cluster formula[a]	Core	Staple	Ref.
1	$[Au_{23}(c\text{-}C_6)_{16}]^-$	Au_{15}	$2[Au_3(SR)_4]$, $2[Au(SR)_2]$ and 4 bridging (-SR-)	102
2	$Au_{25}(PET)_{18}$	Au_{13}	6(RS-Au-SR-Au-SR)	100
3	$[N(C_8H_{17})_4][Au_{25}(PET)_{18}]$	Au_{13}	6(RS-Au-SR-Au-SR)	90
4	$Au_{28}(SPh\text{-}tBu)_{20}$	Au_{20}	4(-SR-Au- SR-Au-SR-) and 8 bridging (-SR-)	103
5	$Au_{36}(SPh\text{-}tBu)_{24}$	Au_{28}	4(SR-Au-SR-Au-SR) and 12 bridging (-SR-)	104
6	$Au_{38}(PET)_{24}$	Au_{23}	3(RS-Au-SR) and 6(RS-Au-SR-Au-SR)	105
7	$Au_{102}(p\text{-}MBA)_{44}$	Au_{39}	$2[RS\text{-}(AuSR)_2]$ and 19(RS-Au-SR)	106
8	$Ag_{14}(SC_6H_3F_2)_{12}(PPh_3)_8$	$(Ag_6)^{4+}$	$8[Ag^+(SC_6H_3F_2^-)_2PPh_3]$ tetrahedra sharing one $(SC_6H_3F_2^-)$ between them	107
9	$Ag_{16}(DPPE)_4(SPhF_2)_{14}$	$(Ag_8)^{6+}$	$[Ag_8(DPPE)_4(SPhF_2)_{14}]^{6-}$	108
10	$[PPh_4]_2[Ag_{32}(DPPE)_5(SPhCF_3)_{24}]$	$(Ag_{22})^{12+}$	$1[Ag_6(DPPE)_3(SPhCF_3)_{12}]^{6-}$, $2[Ag_2(DPPE)(SPhCF_3)_4]^{2-}$ and $4(SPhCF_3)^-$	108
11	$Na_4Ag_{44}(p\text{-}MBA)_{30}$	$Ag_{12}@Ag_{20}$ two shell core	$6[Ag_2(SR)_5]$	109
12	$[PPh_4]_4[Ag_{44}(SPhF)_{30}]$	$Ag_{12}@Ag_{20}$ two shell core	$6[Ag_2(SR)_5]$	110

[a] Abbreviations used are p-mercaptobenzoic acid (p-MBA), phenylethane thiol (PET), 4-tertbutylbenzenethiol (SPh-tBu), triphenylphosphine (PPh_3), diphenylphosphinopyridine (PPh_2Py), 4-fluorothiophenol (SPhF), 3,4-difluorothiophenol ($SPhF_2$), 4-(trifluoromethyl)thiophenol ($SPhCF_3$), 1-cyclohexanethiol (c-C_6), 1,2-bis(diphenylphosphino)ethane (DPPE).

staples of the kind $M(SR)_2$, $M_2(SR)_3$, $M_2(SR)_5$, *etc.* where M = Au, Ag. The structural aspects of these clusters are described using the "divide and protect" concept suggested by Hakkinen *et al.*[101] The clusters may be considered to be composed of a core and distinct number of specific staples. Table 1 summarizes this concept.

Now, coming to mass spectrometry, it can give not only the information about core sizes but also the ligand composition.[9,10,26] Along with this, some metals like silver (Ag) and palladium (Pd) have several isotopes which results in broad isotopic distribution in the mass spectrum. So, assignment becomes much more precise. Fragmentation of ligands or the metal–ligand bond can create some problem in assignments but in most of the cases, that can be overcome by optimizing the mass spectral conditions. Several advances have happened in the recent past to improve the quality of mass spectrum of nanoclusters.

3.1 Au clusters

Among the clusters reported so far, gold clusters have been studied extensively.[19,23,47,91,92,95] This is mainly because of the high stability of such clusters under ambient conditions. Although a few of them, such as Au_{23},[102] Au_{25},[90,100] Au_{28},[103] Au_{36},[104] Au_{38}[111] and Au_{102},[106] have been crystallized, the chemical composition of most of them has been

assigned based on mass spectrometry. ESI MS and MALDI MS and in a few cases LDI have been utilized to assign the composition precisely. Being a softer technique, ESI MS works well for aqueous soluble gold clusters but for organic soluble clusters such as alkanethiol protected ones (which are the most commonly used ligands as they are known to generate stable gold clusters), this technique is not well suited. This is because of very poor ionizing capacity (either in positive or in negative mode) of such clusters. Several new strategies have been followed to get rid of this problem, such as ligand exchange or adding some external ionizing agents *etc*. Ligand exchange with some good ionizable ligands often results in nice mass spectral features.[35] Tsukuda *et al.* have introduced oxidation (by $Ce(SO_4)_2$) or reduction (by $NaBH_4$) to improve the ionizing capacity by enhancing the charge on the Au_{25} cluster.[112] Jin *et al.* have found an external ionizing agent, Cesium (CsOAc) acetate to enhance the ionization (Fig. 4).[31] This works well with the alkane or phenyl substituted ligands and most importantly in this process mass spectrum of bigger clusters such as Au_{333} is also achievable (Fig. 4). Fields-Zinna

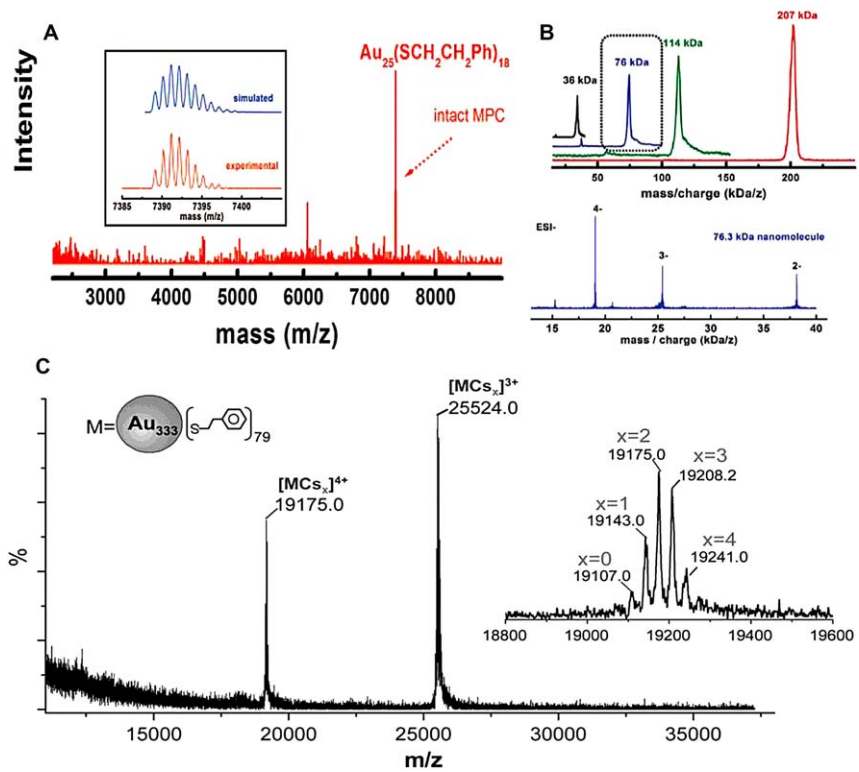

Fig. 4 (A) Positive MALDI MS data of $Au_{25}(SCH_2CH_2Ph)_{18}$ cluster. Inset shows the expanded spectrum plotted along with the calculated spectrum (blue trace). Reproduced with permission.[9] ©ACS publishing. (B) MALDI MS of a 76.3 kDa cluster along with 36, 114, and 207 kDa clusters (above). ESI MS of purified 76.3 kDa clusters (below). Reproduced with permission.[44] ©ACS publishing (C) ESI MS of $Au_{333}(SCH_2CH_2Ph)_{79}$ cluster. Inset shows the expanded mass spectrum of the peak at $m/z = 19\,175.0$. ©PNAS publishing. Reproduced with permission.[31]

has introduced quaternary amine ligand as an external ionizing agent to get a better signal. But most of the clusters do not ionize with all these. For those cases, MALDI MS works better but it is always important to use a suitable MALDI matrix. Usually, weak organic acids such as sinapinic acid, cinamic acid, *etc.* have been used as matrices, but the problem with these matrices is that they do not prevent the fragmentation. In 2008, Dass *et al.* showed that *trans*-2-[3-(4-*tert*-butylphenyl)-2-methyl-2-propenylidene] malononitrile (DCTB) works well for Au clusters (Fig. 4).[9] They have shown its effectiveness for all range of particles starting form 5 kDa to 76 kDa (Fig. 4B).[44] A comparative MALDI MS data of $Au_{25}(PET)_{18}$ using several matrices is given in Fig. 5 which shows the effectiveness of DCTB as a matrix for such clusters. The main reason for the success of this matrix is that it ionizes the molecule by electron transfer whereas in other cases it is proton transfer that serves ionization. Although the technique has been greatly used for organic soluble clusters for hydrophilic ligands, it is not suitable as they tend to form fragments under laser irradiation.

3.2 Silver clusters

Silver clusters are the widely studied noble metal clusters next to Au. Many clusters with various metal cores like Ag_7,[113] Ag_8,[113] Ag_9,[114] Ag_{32},[18,36] Ag_{44},[5,22,109,110,115] Ag_{152},[41] *etc.* have been synthesized through various techniques like interfacial synthesis, solution phase and solid phase

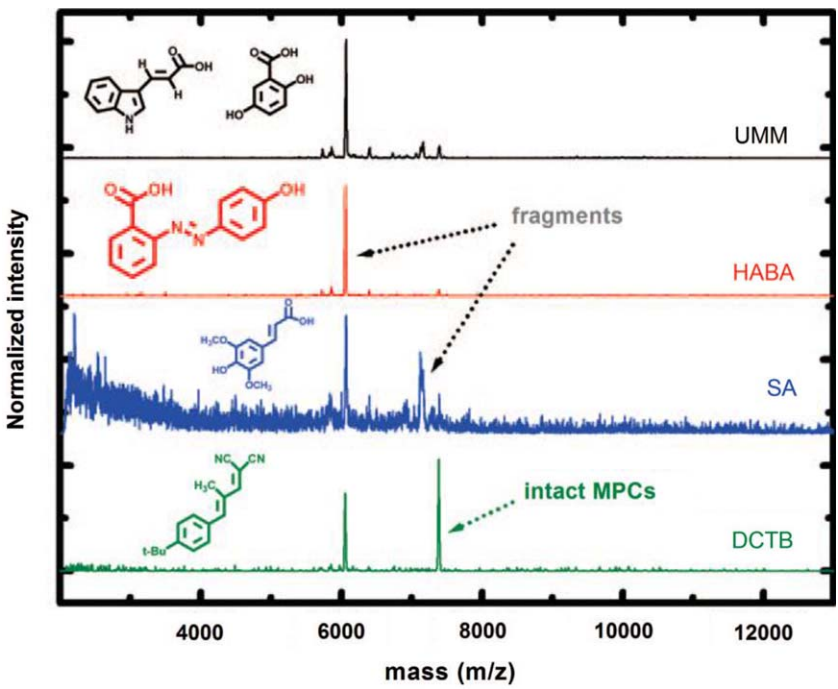

Fig. 5 MALDI MS spectra of $Au_{25}(SCH_2CH_2Ph)_{18}$ using different matrices. The matrices are universal maldi matrix (UMM – 1 : 1 mixture of dihydroxybenzoic acid and α-cyano-4-hydroxycinnamic acid), 4′-hydroxy-azobenzene-2-carboxylic acid (HABA), sinapinic acid (SA) and DCTB. Their structures are shown above the traces. ©ACS Publishing. Reproduced with permission.[9]

synthetic protocols. Although single crystal XRD would have been the best method for identifying any cluster core structure, the inability to crystallize these clusters because of their poor stability makes mass spectroscopic techniques important in their identification.[109,110] Most of the analysis of these clusters have been done through MALDI MS, ESI MS, and LDI MS. Rao *et al.* reported mercaptosuccinic acid (H_2MSA) protected Ag_7,[113] Ag_8,[113] and Ag_9[114] clusters, the former two were synthesized *via* an interfacial etching reaction between an aqueous/organic (toluene) interface and the latter by a solid state synthetic technique. All of these clusters were studied thoroughly and their compositions were assigned precisely by ESI and MALDI MS studies. In yet another example, the power and scope of mass spectrometry has been shown by Guo *et al*. by proper identification of $Ag_{32}(SG)_{19}$(SG = glutathione) cluster using ESI MS technique by optimizing various parameters like source temperature, trap/transfer collision energies and cone gas flow rate (for improved collisional cooling).[18] The nature of the solvent also proved to be a parameter in making mass spectrometry a powerful tool in identifying this silver cluster.[18] Chakraborty *et al.* have shown the effectiveness of MALDI MS for the identification of $Ag_{152}(SCH_2CH_2Ph)_{60}$ cluster where a sharp peak at *m*/*z* 24600 was seen along with a dication at *m*/*z* 12300 (Fig. 6A).[41] The high stability of this cluster is because of the closed shell electronic structures (92 electron system). Emergence of metallicity has also been investigated for a range of silver clusters identified through MALDI MS with DCTB as the matrix.[40] Harkness *et al.* have identified the $Ag_{44}(SR)_{30}$ clusters in 2012[22] which was found to be the most stable silver cluster among all and its crystal structure has also been solved recently.[109,110] The HRESI spectra of 4-flurothiophenol and 2-naphthalenethiol protected Ag_{44} clusters show exact matching with the corresponding calculated spectra (Fig. 6B). Similarly, selenolate protected Ag_{44} cluster (Fig. 6C) also shows features for the 2-. 3- and 4- ions. Thus mass spectrometry has been effective for determining the composition of silver clusters.[42]

4 Multidimensional mass spectrometry

Diverse multidimensional techniques such as MS/MS and ion mobility mass spectrometry (IMS) have been utilized for better understanding of such atomically precise pieces of matter. A brief discussion is given below.

4.1 MS/MS

Mass spectrometric characterization of clusters is often incomplete without MS/MS. Conducting such studies at high masses typical of clusters is difficult in most of the mass spectrometers. However, due to the multiple charges present on clusters, these studies become possible in most of the quadrupole instruments coupled with TOF, as the quadrupole analyzers can select mass and TOF can do mass analysis of the product ions. Limited MS/MS is possible in other instrument configurations such as reflectron and TOF TOF instruments; these

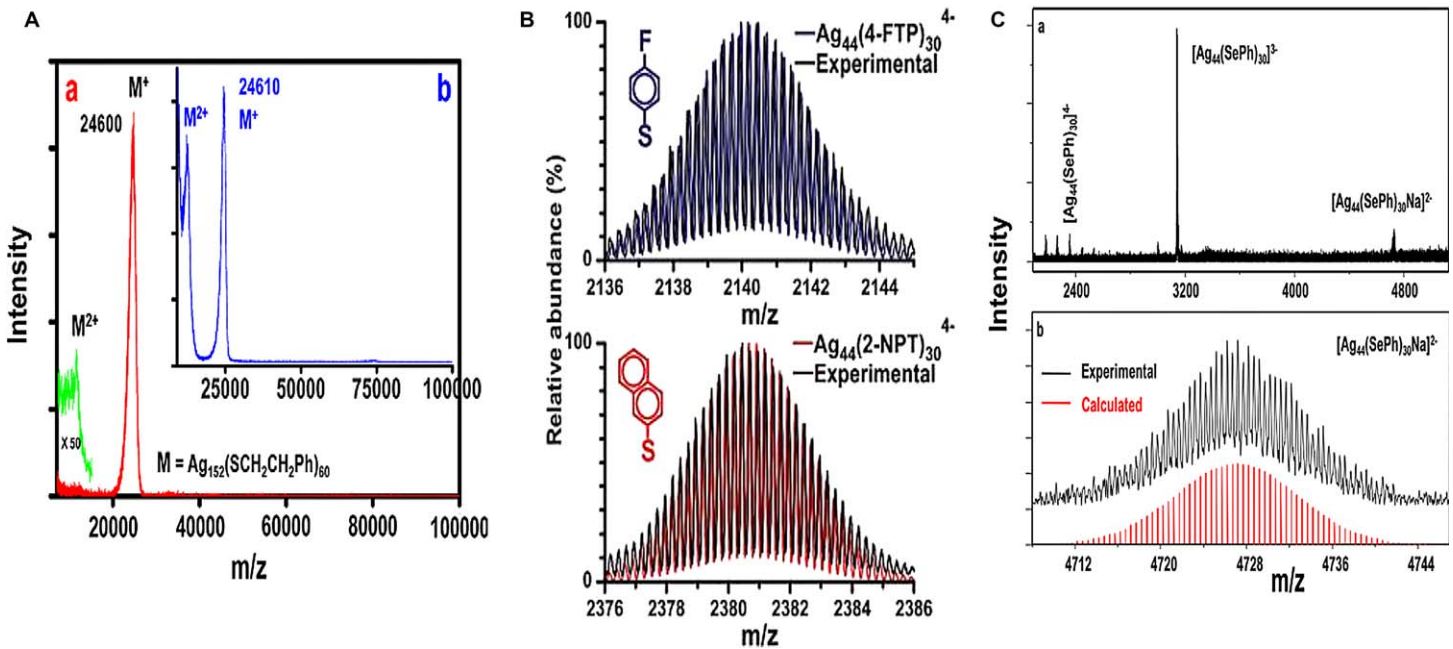

Fig. 6 (A) MALDI MS of as-synthesized $Ag_{152}(SCH_2CH_2Ph)_{60}$ cluster detected in the positive mode. Inset shows the mass spectrum of Ag_{152} cluster purified using HPLC. ©ACS publishing. Reproduced with permission.[41] (B) Mass spectra of $Ag_{44}(SC_6H_4F)_{30}^{4-}$ and $Ag_{44}(SC_{10}H_7)_{30}^{4-}$ clusters plotted along with the corresponding calculated spectra. ©RSC publishing. Reproduced with permission.[22] (C) a) HRESI MS of as-synthesized $Ag_{44}(SePh)_{30}$ cluster taken in negative mode which shows clear 2-, 3- and 4-ions of the same. b) Expanded mass spectrum of the 2- ion plotted with simulated spectrum. ©ACS publishing. Reproduced with permission.[42]

measurements, however, may not be called MS/MS as mass selection is incomplete. Due to the reduced isotope resolution, in view of the large mass, precise characterization is difficult, although several attempts have been made to do the same. In the following examples, we present a few results for MS/MS studies. Ghosh *et al.* showed in an MS/MS study that fragmentation of $Au_{18}SG_{14}$ gives closed shell ions with 8 electrons,[15] this suggests that the number of electrons in the ligand is also important in deciding the electronic structure of the cluster, determining its stability. MS/MS has been used to understand the composition of clusters especially in cases where the metal contains a rich isotope distribution. This has again been demonstrated by Wu *et al.* where the fragmentation pattern of $Ag_7(DMSA)_4$ obtained from MS/MS was analysed in a detailed fashion confirming a closed shell ion with 4 electrons.[38] Ghosh *et al.*'s study in Fig. 7A) shows the ESI MS data of the $Au_{18}SG_{14}$ cluster where four prominent peaks at *m*/*z* 1956.2, 1565.2, 1304.3, and 1117.4 were observed

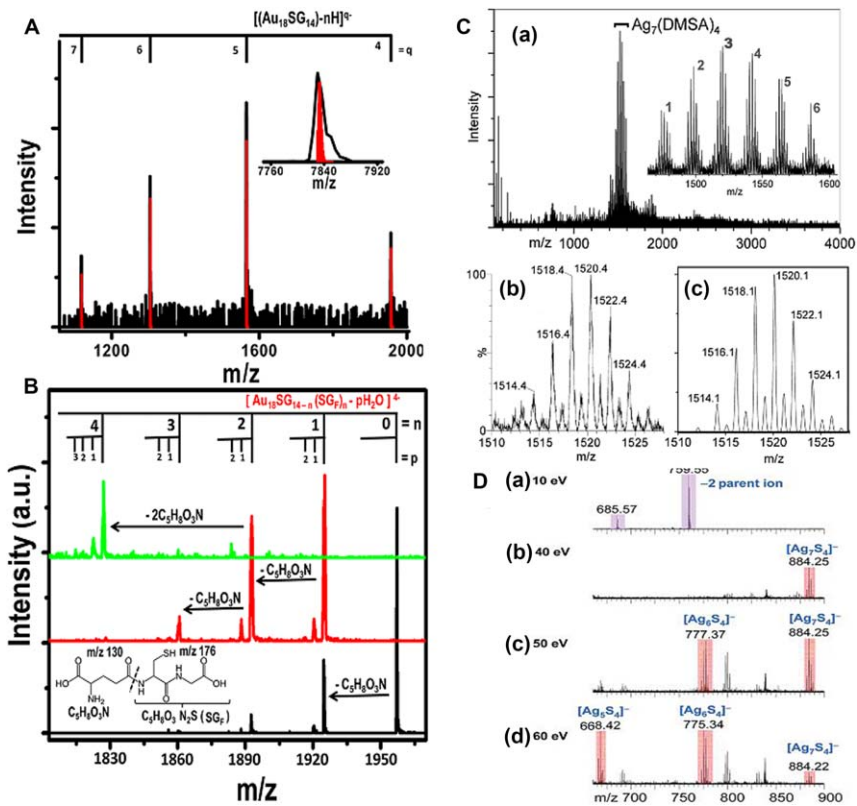

Fig. 7 (A) ESI MS of $Au_{18}SG_{14}$ in the negative mode. The deconvolated spectrum is shown as the inset along with the expected mass peak for $Au_{18}SG_{14}^{-}$. (B) MS/MS spectra of $[Au_{18}SG_{14}]^{4-}$ with increasing collision energy. Inset shows the fragmentation channel of glutathione. The mass spectra from bottom to top are with increasing collision energy. Reproduced with permission.[15] ©ACS Publishing. (C) ESI MS of silver clusters (negative ion mode, inset shows the zoomed-in spectrum as shown in a). (b) and (c) show the experimental and simulated isotopic pattern of $Ag_7L_4 - 2H + 2Na$. (D) MS/MS analysis of the clusters (dianion $[Ag_7L_4 - 3H + 2Na]^{2-}$). ©ACS Publishing. Reproduced with permission.[38]

corresponding to four different charge states of the cluster ($q = 4$, 5, 6, and 7). MS/MS study of the 1956 peak (Fig. 7B) showed fragment peaks with a separation of m/z 32.5 predicting the possible loss of a fragment of mass 130 ($32.5 \times 4 = 130$) which can only arise from the –SG ligand when the $C_{glutamic\ acid} - N_{cysteine}$ bond cleaves giving rise to two fragments of $m/z = 130$ ($C_5H_8O_3N$) and 176 ($C_5H_8O_3N_2S$). The data showed a systematic loss of $C_5H_8O_3N$ as the collision energy was increased. The data showed a series of peaks separated at $m/z = 4.5$ corresponding to the loss of H_2O ($4.5 \times 4 = 18$) indicating that glutathione existed as an anhydride at the surface of the fragment.

Most of the clusters have not been examined by MS/MS also due to poor ion intensity. Clusters being metastable undergo facile fragmentation and obtaining molecular ions at high intensity for MS/MS analysis has been possible only in a few cases. The routine fragmentation pattern, namely ligand loss is seen only in a few cases as the neutral M-L species are more stable leading to their losses. The product cluster formed is often not electronically stable, leading to additional fragmentation, making it impossible to identify them. The foregoing suggests that routine MS/MS examination of clusters require the development of new ionization methodologies.

4.2 Ion mobility mass spectrometry (IMS)

New techniques have been introduced into commercial mass spectrometers for better understanding of the structural features of a molecule. Ion mobility mass spectrometry is an example of that which has been used for different ligand protected gold nanoparticles to understand several aspects of its structure in the gas phase.[19–21] The principle of this technique is to separate specific ions based on their size, more prominently ion surface area. In short, in this mass spectrometer, ions are injected into a gas-filled drift tube where they experience numerous low-energy collisions with a background gas and that separates ions based on the ion-neutral collision cross section (CCS).[19] Just like liquid chromatography, here also smaller ions elute faster than larger ions which experience more collisions. In most of the cases IMS has been used to understand the size of gold nanoparticles but it also helps to understand the fragments generated from them such as $Au_4(SR)_4$ which are often seen in the mass spectrum of $Au_{25}(SR)_{18}$. The same was found for the case of $Au_{38}(SCH_2CH_2Ph)_{24}$ and $Au_{68}(SCH_2CH_2Ph)_{34}$.[43] But from crystal structure, no such species has been found as a staple which does suggest that this fragment is generated in mass spectral conditions. Even Fields-Zinna *et al.* have found that in tandem mass spectrometric conditions tetrameric ion, $NaAu_4(SR)_4^+$ can be generated from $Au_{25}(SR)_{18}$ clusters.[14] In IMS, one can reduce such fragmentations and one can reduce the noise to get a low intense peak in a much prominent way. Dass *et al.* have done the IMS study of $Au_{25}(SCH_2CH_2Ph)_{18}$ cluster where they have shown that it is possible to distinguish between the fragmentation of the core as well as shell which consist of six [-SR-Au-SR-Au-SR-] staples. Along with the predominant $Au_4(SR)_4$, other smaller fragments such as $Au(SR)_2^-$, $Au_2(SR)_3^-$, $Au_3(SR)_4^-$, and $Au_4(SR)_5^-$ were also seen.[6]

5 Clusters of other metals

Compared to the vastly studied and rapidly growing field of monolayer protected clusters of Au and Ag, clusters of other metals are in their infancy. There are only a few reports of clusters of metals like Pd, Cu, Pt, *etc.*, and some alloy clusters of these metals with Au and Ag have been studied up to an extent. This section gives a brief account of mass spectrometric investigation of clusters of metals like Pd, Pt, Cu and of a few alloy clusters.

5.1 Pt clusters

There are several attempts to create fluorescent Pt nanoclusters by different methods. Giuffrida *et al.* developed a methodology to obtain ultrasmall, water-soluble, carboxylate-terminated Pt clusters.[116] Yuan *et al.* have synthesized highly fluorescent Pt clusters employing mild etching process by phase transfer *via* electrostatic interaction.[117] There are also reports on blue[118] and yellow emitting Pt clusters[119] protected by thiol, thioether and ester – functionalized polymer and glutathione. But we will not go in to the details of synthesis of these materials and will focus on their mass spectrometry.

The Pt clusters made up of 4 to 6 Pt atoms protected by *N,N*-Dimethylformamide were synthesized by Kawasaki *et al.* by previously reported process. These clusters were photo – luminescent with their emission maximum dependent upon the excitation wavelength. The composition of these clusters was determined by MALDI MS by ligand exchanging them with 2-mercapto-benzothiazole (MBT). The mass spectrum shown in Fig. 8A, consisted of a peak corresponding to $Pt_5(MBT)_7$ as the dominant signal and it was in agreement with the simulated mass obtained in isotopic analysis. The clusters with 4 and 6 Pt atoms were also present which were assigned as shown in the Fig. 8A.[120]

Recently, a blue emitting 11-atom Pt cluster protected by 4-(*tert*-butyl)benzylmercaptan (BBSH), $Pt_{11}(BBS)_8$ was reported.[8] The cluster was synthesized by the solid state method wherein H_2PtCl_6 and BBSH were ground to form thiolates first and these thiolates were reduced using appropriate quantity of $NaBH_4$. The molecular formula of clusters was assigned using MALDI MS and ESI MS data, shown in Fig. 8B. The main figure shows the MALDI mass spectrum obtained at threshold laser power using the DCTB matrix. The peak was observed to be broader compared to that of the $Au_{25}PET_{18}$ cluster. This is mainly because Pt has five isotopes (^{192}Pt, ^{194}Pt, ^{195}Pt, ^{196}Pt and ^{198}Pt) and Au has only one (^{197}Au). So FWHM of the Pt cluster is larger than that of Au clusters. There are also other reasons like laser induced fragmentation increasing the broadness of the peak. ESI MS of the cluster is shown in inset of Fig. 8B with simulated spectrum showing agreement with the $Pt_{11}(BBS)_{18}$ formula. The ESI MS was measured in 1 : 1 mixture of toluene-methanol in positive ion mode. CsOAc was used as ionization enhancer as ligand was completely non-polar. The peak at $m/z = 3730$ was assigned to $[Pt_{11}(BBS)_8Cs(H_2O)]^+$ ion.[8]

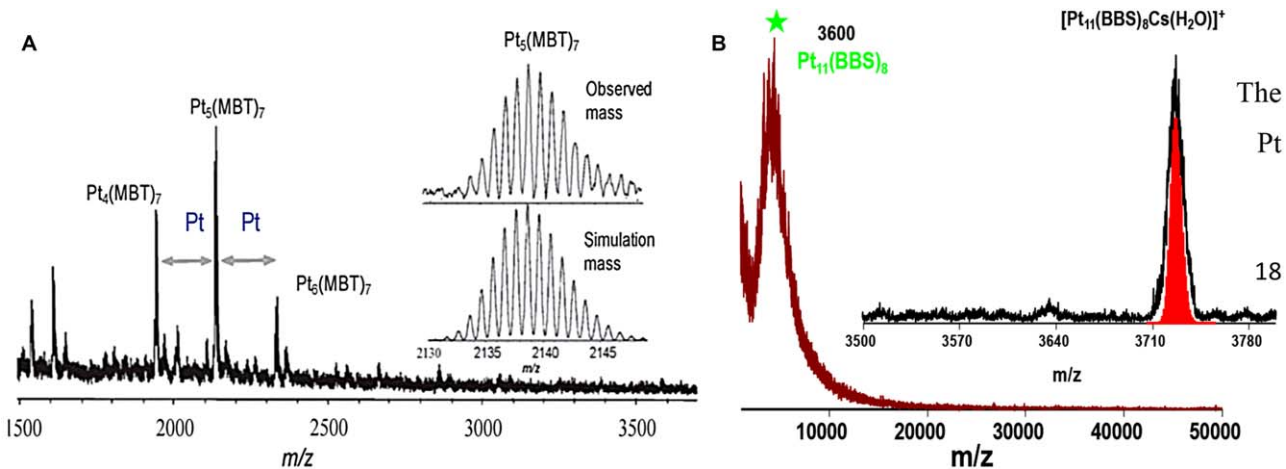

Fig. 8 (A) Negative-ion MALDI MS of MBT protected Pt clusters prepared by ligand exchanging DMF-protected clusters with MBT. The observed and simulated isotopic distributions of the peak with highest intensity show a good agreement with assigned composition $Pt_5(MBT)_7$. The peaks corresponding to $Pt_4(MBT)_7$ and $Pt_6(MBT)_7$ were also observed. Reproduced from Ref. 120 with permission from The Royal Society of Chemistry. (B) MALDI MS of Pt cluster protected by BBSH observed at threshold laser power using DCTB matrix with inset showing ESI MS of the cluster obtained using CsOAc as enhancer, plotted with the simulated spectrum (shaded) for the corresponding composition. Based on the MALDI MS and ESI MS data the cluster was assigned to be $Pt_{11}(BBS)_8$. Reproduced from Ref. 8 with permission from The Royal Society of Chemistry.

5.2 Pd clusters

Though there are several reports on the synthesis and characterization of Pd clusters,[121–125] mass spectrometric investigations of them are rare. TEM has been used as a major characterization tool in all these cases.

Negishi *et al.* synthesized Pd clusters by reacting $PdCl_2$ with alkanethiols, RSH (R = *n*-$C_{18}H_{37}$, *n*-$C_{12}H_{25}$). They analysed chemical composition of the clusters formed by mass spectrometry using a MALDI TOF apparatus constructed in their group in the presence of anthracene as the matrix. They observed $Pd_5(SC_{18}H_{37})_{10}$ and $Pd_{10}(SC_{18}H_{37})_{12}$ thiolate complexes as the major species and also peaks corresponding to some other fragment ions formed during the MALDI process, in positive mode, when the sample was diluted by anthracene to $\sim$1 mol%.

They have also observed significant dependence of mass spectral features on the relative concentration of sample and matrix. When the sample was diluted to 20 mol% by anthracene, the peaks were not assignable to any combinations of Pd and $C_{18}H_{37}SH$, but to $Pd_nS_m^+$ and peak positions were independent of chain length of the ligand. Thus they came to a conclusion that samples contained Pd : SR clusters designated as $Pd_n(SR)_m$ and that all the C–S bond cleavage was induced because of UV absorption by clusters, efficiently and selectively.[126]

5.3 Cu clusters

Wei *et al.* demonstrated the synthesis of small Cu_n clusters ($n \leq 8$) in solution following a single phase wet chemical route. These clusters were protected by 2-mercapto-5-*n*-propylpyramidine (MPP) ligand. The chemical composition of these clusters was determined using ESI MS as the major characterization technique. The ESI mass spectrum recorded in the positive ion mode is shown in Fig. 9A. The highest mass peak at $m/z = 1120$ was found to be corresponding to Cu_8L_4 (L = $C_7H_9N_2S$). Other fragments like Cu_8L_3 ($m/z = 1015$), Cu_6L_4 (995), Cu_5L_4 (978), Cu_8L_3 (968) and Cu_5L (470) were also present in the mass spectrum.[127]

A sub-nanometer Cu cluster protected by benzotrizolate (BTA), Cu_nBTA_m was reported by Salorinne *et al.* in 2012. They synthesized these clusters by following the single-phase Brust – Schiffrin protocol in methanol, which involves two steps that are 1) formation of benzotriazolate – Cu(II) complex and 2) reduction of Cu(II) ions to Cu(0) by the addition of $NaBH_4$. The mass spectral features of these clusters were studied by ESI MS, both in positive and negative mode by diluting a DMF dispersion of the clusters with acetonitrile (positive – mode spectrum is shown in Fig. 9B). Two major peaks were observed at $m/z = 607.8$ and 788.8 which were assigned to Cu_4L_3 and Cu_5L_4, respectively (L = BTA). The smaller peaks at $m/z = 648.8$ and 696.7 were identified as solvent adducts of Cu_4L_3 and Cu_4L_3O species. Some organic fragments and fragments containing one Cu atom were found in the lower mass region. In the negative mode only the smaller species, such as, CuL_2 and BTA anions were present and clusters were no longer found.[32]

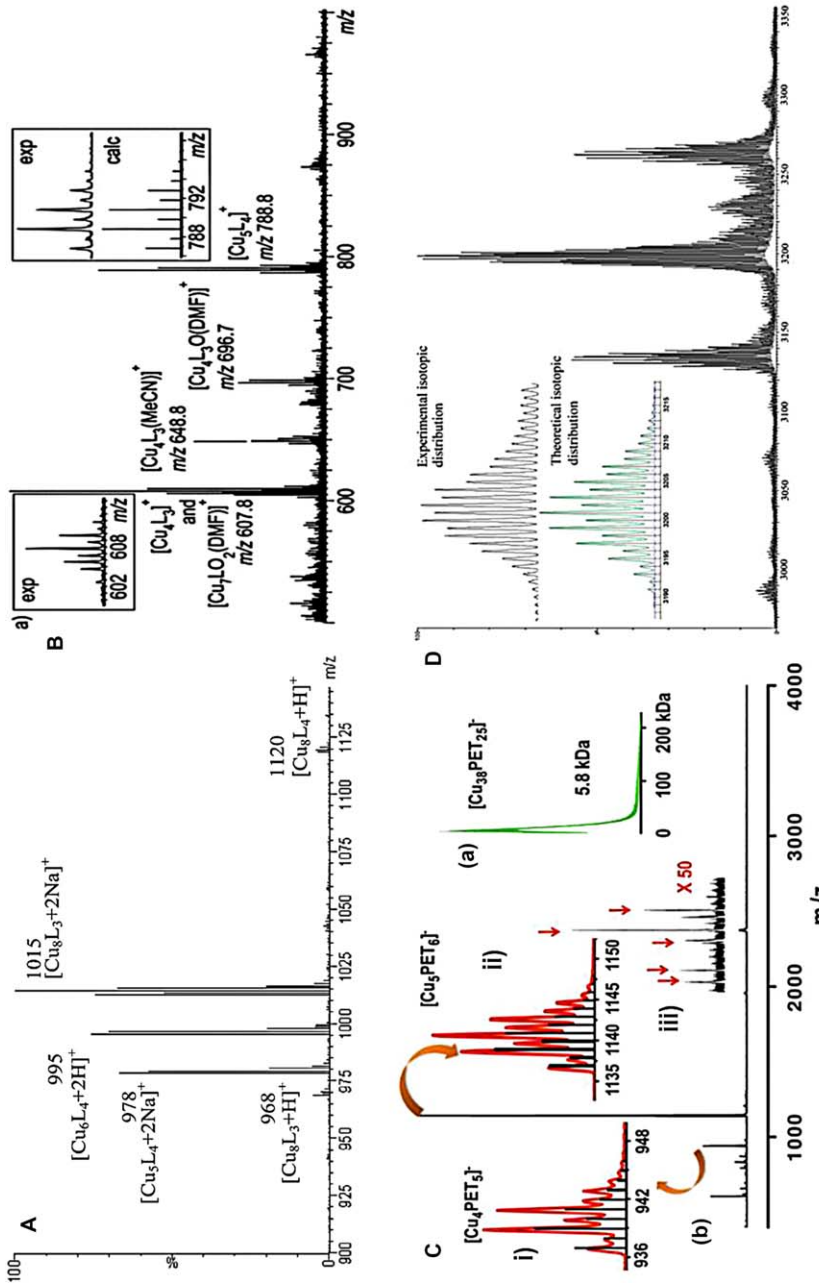

One more Cu cluster protected by 2-phenylethanethiol (PET) was reported in 2013.[45] It was prepared by following the solid – state route. In order to find the molecular composition of these clusters, both MALDI MS and ESI MS characterization of the material was performed. MALDI MS was obtained in the negative mode using DCTB as the matrix which showed a single peak at around $m/z = 5800$ which was assigned to $\sim Cu_{38}(PET)_{25}$ (shown in Fig. 9C(a)). There was only a single peak in MALDI MS showing the existence of a single species. The ESI MS data of clusters obtained in the negative mode is shown in Fig. 9C(b). The molecular ion features were not observed in ESI MS, but peaks corresponding to some fragment ions could be seen. The peaks with maximum intensity at $m/z = 1141$ and 941 were assigned to the fragments $[Cu_6(PET)_5]^-$ and $[Cu_5(PET)_4]^-$, respectively and experimental and theoretical isotopic distributions are shown in insets of Fig. 9C(b). The other peaks identified were at $m/z = 2655$, 2459, 2359, 2124 and 2056 and these were assigned to the fragment ions, $[Cu_{34}(PET)_{23}]^{2-}$, $[Cu_{30}(PET)_{22}]^{2-}$, $[Cu_{29}(PET)_{21}]^{2-}$, $[Cu_{28}(PET)_{23}]^{2-}$ and $[Cu_{28}(PET)_{17}]^{2-}$, respectively which are indicated by arrows in inset iii of Fig. 9C(b). These fragments compliment the presence of PET-protected copper clusters in solution.[45]

An unprecedented 20 atom copper cluster incorporating 11 hydrides into the system with a molecular formula, $Cu_{20}H_{11}(S_2P(O^iPr)_2)_9$ was reported by Liu *et al.* The cluster was synthesized in tetrhydrofuran (THF) by reaction of a mixture of $NH_4[S_2P(O^iPr)_2]$ and $[LiBH_4.thf]$ with $Cu(CH_3CN)_4PF_6$ and positive ion ESI MS was carried out to determine its chemical composition. The spectrum obtained is shown in Fig. 9D. The peak with highest intensity at $m/z = 3198.5$ was assigned to the molecular ion. The peaks at $m/z = 3132.6$ and at $m/z = 3262.3$ were assigned to the fragment $[C_{19}H_9(S_2P(O^iPr)_2)_9]^+$ and adduct $[Cu + Cu_{20}H_{11}(S_2P(O^iPr)_2)_9]^+$, respectively. The cluster was crystallized and the structure of the cluster was determined by single – crystal X-ray diffraction (XRD) studies. It consists of an elongated triangular orthobicupola framework of 18 Cu atoms encapsulating a $[Cu_2H_5]^{3-}$ ion.[128]

Fig. 9 (A) ESI MS of MPP protected copper clusters in the positive ion mode. The highest mass peak at $m/z = 1120$ is assigned to Cu_8L_4 ($L = C_7H_9N_2S$) and other peaks in lower mass range correspond to the fragments described in the text. Reproduced with permission.[127] ©ACS Publishing. (B) ESI MS-TOF mass spectrum of copper clusters protected by BTA in positive mode measured using DMF dispersion of clusters diluted with acetonitrile. The inset (on the right hand side) shows the experimental and calculated isotopic distribution of the peak at $m/z = 788.8$ due to Cu_5L_4. The other inset (on the left hand side) shows the expanded view of the peak at $m/z = 607.8$ assigned to Cu_4L_3. ©RSC Publishing. Reproduced with permission.[32] (C) a) MALDI MS of the PET protected Cu clusters measured in linear negative ion mode, measured using DCTB matrix. The single peak in the spectrum shows the presence of single species with the composition, $Cu_{38}PET_{25}$. b) ESI MS measured in negative mode with insets showing observed and calculated (black) spectra corresponding to i) $[Cu_4(PET)_5]^-$ and ii) $[Cu_5(PET)_6]^-$ species and iii) expanded (Y axis) view of a selected region showing fragments mentioned in the text. ©Springer Publishing. Reproduced with permission.[45] (D) ESI MS of $Cu_{20}H_{11}(S_2P(O^iPr)_2)_9$ cluster in positive mode with inset showing the observed and calculated spectra for molecular ion peak. The peak at lower mass is attributed to the fragment and that at higher mass is attributed to a Cu adduct of the molecular ion which are described in the text. ©ACS Publishing. Reproduced with permission.[128]

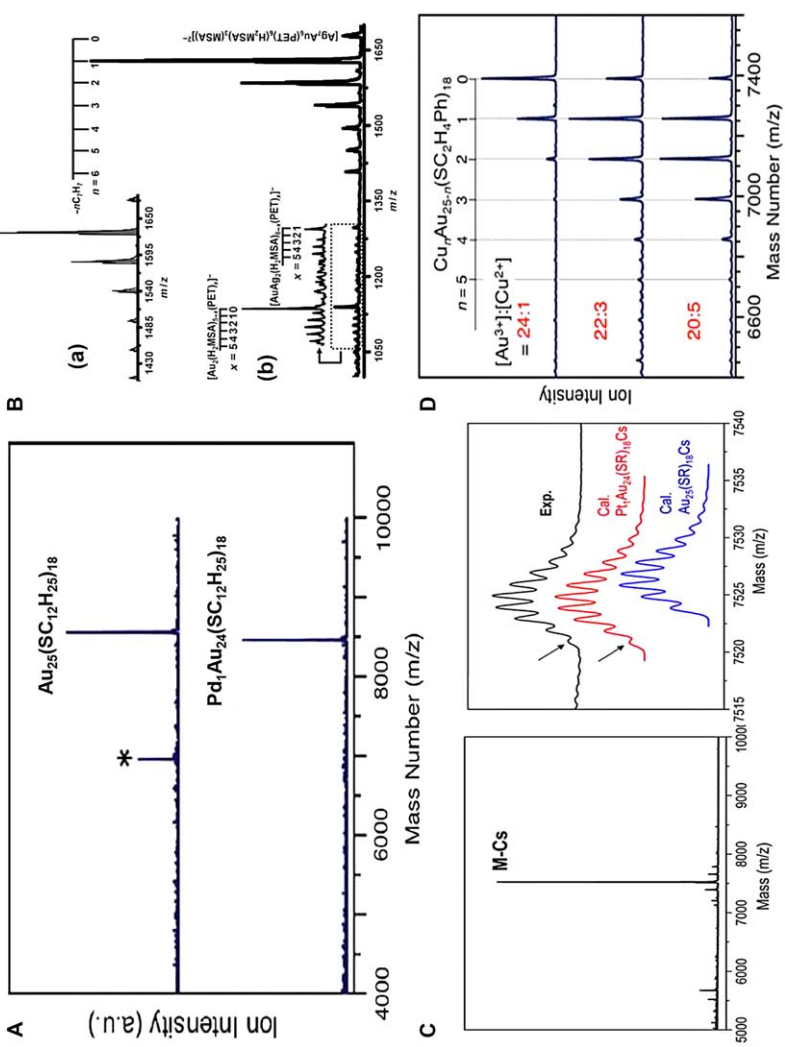

5.4 Alloy clusters

Alloy clusters, also referred to as alloy nanoclusters or nanoalloys are composed of atoms of two or more elements in definite compositions. Alloy clusters with a wide range of combination of elements and different compositions are known till date; some of them are $Au_{24}Pd$,[12,46] $Au_{36}Pd_2$,[129] $Au_{24-n}Ag_n$ series,[130] $Au_{24-n}Cu_n$ series,[131] $Au_{24}Pt$,[132] Ag_4Ni_2,[133] *etc.* Due to alloying, we can observe an enhancement in specific properties of clusters because of synergistic effects. Also due to rich diversity in compositions, structures and properties, they find widespread applications in different fields.[134] Some examples of these will be discussed here with more emphasis on their mass spectrometry.

Murray *et al.* reported the monopalladium doped bimetallic cluster, $Au_{24}PdL_{18}$ (L = 2-phenylethanethiol) in 2010. Their synthesis procedure was similar to that of $Au_{25}PET_{18}$, but they used mixture of Au and Pd salts instead of gold salt ($HAuCl_4$) alone. They confirmed the mono-Pd doping by ESI MS of clusters, partially ligand exchanged with thiolated(polyethlyneglycol) (PEG), and also with MALDI TOF MS analysis.[13] Negishi *et al.* isolated highly pure dodecanetiolate – protected $Au_{24}Pd$ cluster using solvent fractionation and high-performance liquid chromatography (HPLC). The negative ion MALDI mass spectrum of purified cluster as compared to that of $Au_{25}(SC_{12}H_{25})_{18}$ is shown in Fig. 10A.[46] The same group reported palladium doped magic number cluster Au_{38} protected by phenylethanethiolate, $Au_{36}Pd_2(SCH_2CH_2Ph)_{24}$, and studied the mass spectral feature of the cluster using MALDI MS and high resolution ESI MS analysis in negative mode. They found that $Au_{37}Pd(SC_2H_4Ph)_{24}$ was also present in solution, but di-palladium doped cluster was more stable compared mono-palladium doped cluster.[129]

The effect of Ag doping on the electronic structure of $Au_{25}(SR)_{18}$ clusters was studied by Negishi *et al.* by considering dodecanethiol as the ligand. The synthesis procedure was similar to that of the Pd-doped cluster. They observed multiple silver atom incorporation into the $Au_{25}(SC_{12}H_{25})_{18}$ system forming a series of clusters, $Au_{25-n}Ag_n(SC_{12}H_{25})_{18}$ ($n = 0$–11), unlike in case of Pd-doping, and that electronic structure of

Fig. 10 (A) The negative mode MALDI MS of $Au_{24}Pd_1(SC_{12}H_{25})_{18}$ cluster along with that of $Au_{25}(SC_{12}H_{25})_{18}$ cluster. The peak highlighted by asterisk corresponds to $Au_{21}(SC_{12}H_{25})_{14}$ fragment. The clusters were purified by HPLC and MALDI MS was collected using DCTB matrix in linear mode TOF mass spectrometer. Reproduced from Ref. 46 with permission from the PCCP Owner Societies. (B) The negative ion ESI MS of the 13-atom alloy cluster Ag_7Au_6 protected by MSA and partially ligand exchanged with PET, in the region $m/z = 1000$–1700. The cluster showed substitution of six MSA ligands by PET which was confirmed by sequential loss of six tropylium ions ($n = 0, 1, 2, \ldots 6$) observed during ionization. The inset a) shows simulated (gray) and observed (black) isotopic pattern of the peaks and b) shows the fragments. Reproduced with permission.[135] ©Wiley-VCH Publishing. (C) ESI MS of $Au_{24}Pt_1(SCH_2CH_2Ph)_{18}$ clusters with experimental and calculated spectra for $[Au_{24}Pt_1(SCH_2CH_2Ph)_{18}Cs]^+$ and $[Au_{25}(SCH_2CH_2Ph)_{18}Cs]^+$ species. The CsOAc was used as ionization enhancer. The most intense peak at $m/z = 7524.8$ was assigned to $Pt_1Au_{24}(SR)_{18}Cs^+$ and assignment was confirmed by isotopic distribution analysis. Reproduced with permission.[132] ©ACS Publishing. (D) Negative mode MALDI MS of $Au_{25-n}Cu_n(SCH_2CH_2Ph)_{18}$ clusters synthesized with precursor salt concentrations $(HAuCl_4)/(CuCl_2) = 24:1$, 22 : 3 and 20 : 5. The peaks observed are assigned to the series, $Au_{25-n}Cu_n(SCH_2CH_2Ph)_{18}$ with n ranging from 0–5 indicated in the figure. ©ACS Publishing. Reproduced with permission.[131]

Au_{25} cluster was continuously modulated by incorporation of each silver atom. The MALDI MS of the clusters in the negative mode contained multiple peaks and all the peaks were assignable to $Au_{25-n}Ag_n(SC_{12}H_{25})_{18}$ ($n = 0$–11). Similar spectra were obtained in positive ion mode as well.[130] In a similar way, doping the magic number cluster, Au_{38} protected by phenylethanethiol, created a series of alloy clusters, $Au_{38-n}Ag_n(SCH_2CH_2Ph)_{24}$, which were characterized by positive ion MALDI TOF analysis.[26] Ag atom incorporation into some other cluster systems like $Au_{144}(SR)_{60}$[25] and $Au_{130}(SR)_{50}$,[136] *etc*., is also reported in the literature resulting in different alloy clusters of Au and Ag. A 13 atom alloy cluster Ag_7Au_6 protected by mercaptosuccinic acid (MSA) was reported by Udayabhaskararao *et al.*[135] These clusters were prepared by the reaction of a mixture of Ag_7 and Ag_8 clusters with $HAuCl_4$ solution. When the ESI MS measurements were done on as – synthesized clusters in aqueous medium no characteristic peaks were observed, because clusters were decomposing due to high capillary temperature of around 313 K. Hence, the clusters were transferred to organic medium by partial ligand exchange of MSA with phenylethanethiol (PET) and ESI MS analysis was performed. The mass spectrum of PET – exchanged clusters is shown in Fig 10B. The peak with highest *m*/*z* was assigned to $[Ag_7Au_6(PET)_6(H_2MSA)_3(MSA)]^{2-}$ and the series of peaks following it correspond to sequential loss of tropylium ion from each PET ligand (*n* in figure indicates the number of tropylium ions lost). The series terminates at six tropylium ion loss confirming the presence of six PET ligands in the system.[135]

The doping of Cu atoms into the $Au_{25}(SCH_2CH_2Ph)_{18}$ system was attempted by Negishi *et al.*, which was reported in 2012. Fig. 10D shows the negative ion MALDI MS of the clusters consisting of multiple peaks, assignable to clusters with different number of Cu incorporation, *i.e.*, $Au_{25-n}Cu_n(SCH_2CH_2Ph)_{18}$ ($n = 0$–5) . Unlike the case of Pd and like in the case of Ag, a series of alloy clusters, $Au_{25-n}Cu_n(SCH_2CH_2Ph)_{18}$ were obtained in this case, which were identified in the mass spectra. But they could observe only up to six Cu atom incorporation and clusters with more than six Cu atoms were hardly observed in experimental conditions followed by them.[131] In case of selenolate protected cluster system, $Au_{25-n}Cu_n(SeC_8H_{17})_{18}$ ($n = 0$–9), up to nine Cu atom incorporation was observed.[137]

Doping $Au_{25}(SCH_2CH_2Ph)_{18}$ clusters with Pt atoms was tried by Jin *et al.* They obtained single Pt doped system, $Au_{24}Pt(SCH_2CH_2Ph)_{18}$. They found that Pt – doping drastically changes the electronic, optical and catalytic properties of clusters. Differentiating Pt (195.08 Da) from Au (196.97 Da) is a tough task because of their very small mass difference (1.89 Da). Hence high – precision ESI MS was used as an analysing tool by them for identifying the new cluster formed. The ESI MS in positive – mode with experimental and simulated spectra are shown in Fig. 10C. Cesium acetate was used as an enhancer in this case and they observed $[Au_{24}Pt(SR)_{18}Cs]^+$ as a major peak at $m/z = 7\,524.8$ Da.[132] The location of Pt atom was later identified by platinum L_3 – edge extended X-ray absorption fine structure (EXAFS) analysis along with X-ray photoelectron

spectroscopy (XPS) and computational analysis. The Pt atom occupies the centre of the icosahedral Au_{13} core.[138]

A bimetallic cluster of Ag and Ni, which involves a noble metal and a first row transition metal, protected by di-mercaptosuccinic acid (DMSA) ligand has been reported in 2012. The cluster was characterized using ESI MS and the structure has been predicted using theoretical calculations.[133]

Thus, mass spectrometry, mainly MALDI MS and ESI MS, has played a major role in identifying clusters of metals like Pt, Pd, Cu and alloy clusters, their composition and structure determination along with other characterization techniques. In case of alloy clusters, mass spectrum is an important tool to know the combination of different metal atoms in a specific cluster.

6 Protein protected clusters

Choice of ligand plays a significant role in cluster science. Starting from gas phase to phosphine and then thiol protection, new era began when people started using macromolecular templates for synthesizing clusters.[139] Peptides,[140] DNA,[141] dendrimer[142] and mostly proteins[139] are the members of this new family. This specific class of molecules bridge materials and biology. In this section we will mostly discuss protein protected clusters. So far several proteins namely, bovine serum albumin (BSA),[28,29,143–152] native lactoferrin (Lf),[39,153] human serum albumin (HSA),[154–156] lactalbumin,[157] pepsin,[158] trypsin,[159] chymotrypsin,[160] lysozyme (Lyz),[161–164] hemoglobin (Hb),[16] horse radish peroxidase (HRP),[165] insulin,[166] *etc.*, have been used for cluster synthesis. Some reports exist on mixed protein matrices used for cluster synthesis such as egg shell membrane,[167] human hair,[168] egg white,[169] *etc.* Along with conventional metals like Au and Ag, several other metals like Pt,[169] Fe,[16] and Cu[17] clusters also have been synthesized using proteins.

Protein protected clusters do not exhibit well defined UV-Vis absorption feature unlike their monolayer protected analogue (as described in the above sections). But they have intense luminescence which allows them to act as sensors for toxic metal ions,[17,39,147–149,151,159,163,170,171] small molecules[143,165,169] and biologically active molecules.[156,162,172] Their luminescence can be used for bio-imaging and bio-labeling.[148,166,173,174] In the context of emerging applications, of biocompatible materials, it is necessary to look into the protein protected clusters in greater details. Although several clusters have been crystallized (see previous section for details) none of the protein protected clusters could be crystallized so far due to the inherent lack of crystallization of proteins in the experimental conditions used for cluster synthesis. Mass spectrometry is an alternate tool for identifying the cluster cores. Proteins are being characterized by mass spectrometry for long and a large body of literature exists on mass spectrometry of proteins and their interaction with other molecules.[11] Many protein protected clusters have been identified by the mass shift in the protein region after cluster synthesis. Typically metal precursors (Au^{3+}/Ag^{+} for Au/Ag clusters) are mixed with

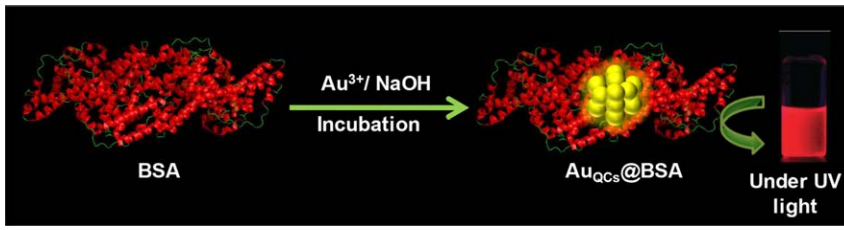

Scheme 1 Schematic representation of protein protected cluster formation taking BSA as an example. The reaction proceeds *via* formation of Au^{+}–protein intermediate adduct. After cluster formation intense red luminescence is observed under UV light.

protein solution to form adducts (Au^{+}-protein/Ag^{+}-protein) which is subsequently reduced to luminescent clusters in presence of a base (for Au as shown in Schematic 1).[150] An external reducing agent namely, $NaBH_4$ is used to synthesize Ag clusters.[28] After cluster formation, protein loses its secondary structure partially (for example, Lyz loses 28% helicity).[17,29,39,161] Fragmentations occur due to the excess base and catalytic fragmentation of the protein occurs by the clusters. These effects ultimately result in poor ionization in ESI MS. To date, none of these clusters could be seen in ESI MS, although, by using latest mass spectrometers we can reach the mass range of bigger proteins like BSA in ESI MS. As a result, mostly these clusters are studied using MALDI MS. In the following sub-sections, we will discuss the mass spectrometric investigations of various protein protected clusters.

6.1 Au, Ag and Au@Ag alloy clusters

MALDI MS is the commonly used technique in this scenario which is a soft ionization method and capable of showing parent singly charged ion, known as the molecular ion. In MALDI MS of protein protected clusters, matrices such as sinapic acid (SA), α-cyano-α-hydroxy cinnamic acid (CHCA), *etc.*, are used.[11] Minimum quantity of cluster solution is mixed well with a larger volume of matrix solution and spotted on the MALDI plate to yield a dried droplet. In 2009, Xie *et al.* first reported mass spectrometric identification of gold clusters protected with BSA.[150] They have shown a mass shift of 25 Au atoms after cluster formation and the cluster was assigned to be Au_{25}@BSA. Note that Au_{25} is one of the magic numbers in clusters. These data were further supported by thermogravimetric analysis. Another magic cluster core, Au_{38}@BSA was prepared by Muhammed *et al.* by core etching of gold nanoparticles.[148] This was also red luminescent. MALDI MS data revealed that only Au_{38} is formed in this process as no other peaks were observed in the higher mass region. Schneider and co-workers proposed the formation of blue luminescent Au_8 core at mild basic conditions (pH 8) and red luminescent Au_{25} core after reducing with ascorbic acid at pH 3. They have used CHCA as the matrix in MALDI TOF and got a Gaussian type of distribution having a series of peaks.[146] Two types of peaks were present, major peaks were separated by m/z 197 due to Au and minor peaks were separated by m/z 32 (from the major peaks) due to sulphur attachment, assuming the formation of $Au_nS_m^{+}$ aggregates. The peaks with maximum intensity were

related to the high population of Au_{22}–Au_{25} cores. Protein structure plays an important role in cluster synthesis. Normally, harsh conditions were used for cluster synthesis and at such conditions proteins change their structure as the structure is highly dependent on pH of the solution used. Predefining the protein structure by controlling the solution pH can help to get different cores as protein structure plays an important role in cluster formation. To prove this hypothesis (tailoring protein structure by controlling solution pH), Yu *et al.* have used CO as a mild reducing agent and maintained the pH of the solution and could isolate five different gold cluster cores (Au_4, Au_8, Au_{10}, Au_{13} and Au_{25}) at different reaction conditions using BSA as the protein of choice.[152] As usual, at high pH (>pH 11) Au_{25} was formed while at mild basic condition (like pH 7.4 maintained using phosphate buffer) smaller cores like Au_{13} were formed (see Fig. 11A). The cores are assigned in terms of mass shift observed in MALDI MS. By changing the Au : BSA concentration at pH 7.4 they could find three smaller cores namely, Au_4, Au_8 and Au_{10} which were confirmed from their respective mass spectra (see Fig. 11B).

There is always some amount of free protein during cluster synthesis. This can be due to excess protein or regeneration of free protein with time (see later for details). Some groups have tried to separate the clusters from excess protein and cluster mixtures. Li *et al.* have dansylated (common green fluorescence tag for proteins which does not change protein conformation) BSA to synthesize the red luminescent clusters. After separation through Sephadex G-75 gel, clusters were collected and the mass spectrum showed the same Au_{25} core.[145] In another approach by Guan *et al.* free BSA was removed from the cluster solution by specific binding with Zn^{2+} ion. After separation, they got only the Au_{25}@BSA peak without free BSA.[175]

Human transferrin has also been used for Au cluster synthesis. Xavier *et al.* through MALDI TOF MS showed a broad distribution of Au nanoclusters ranging from Au_{10}–Au_{55} with peak maxima at 22–33 Au. Between two separate series observed, major peaks are separated by *m*/*z* 197 due to Au and the minor peaks are separated by *m*/*z* 32 due to sulfur.[176]

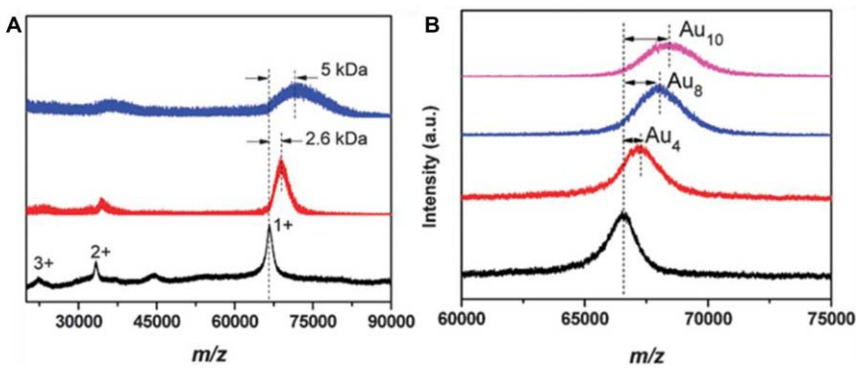

Fig. 11 (A) MALDI MS of Au_4, Au_8 and Au_{10} protected with BSA synthesized at pH 7.4 (using phosphate buffer) by varying BSA to Au ratio from 1 : 5, 1 : 8 and 1 : 12, respectively. Au_{13} and Au_{25} are shown in (B). Au_{13} was prepared at pH 7.4 using BSA : Au ratio to be 1 : 24 while Au_{25} was prepared at pH 11. Reproduced from Ref. 152 with permission from The Royal Society of Chemistry.

Xavier *et al.* have reported the Au_{25} core protected with native (bovine) lactoferrin.[39] They have also identified the intermediate Au_{13} core from the MALDI MS data. They have extended their study to see the evolution of clusters where they have shown that gold ions organize to create the cluster core through aurophillic interactions leading to regeneration of the free protein. We'll discuss this in detail in the following sub-section.

Kawasaki *et al.* have reported synthesis of different cluster cores using pepsin by changing the pH of the system.[158] They have observed red luminescent Au_{25} at pH 12 while Au_{13} forms at pH 1 and blue emitting Au_8 with Au_5 were observed at pH 9. They have used 2-mercaptothiazole (MBA) as well as SA as matrices. They could not find a molecular ion peak for Au_{25}@pepsin but they have assigned the Au_{13} core in the case of green emitting clusters formed at pH 1. Fragmented species like Au_{11}, Au_9, Au_7 and Au_6 were also observed in the mass spec. They have observed that nearest peaks were separated by *m*/*z* 32 due to sulfur and another unknown species with *m*/*z* 177 separation also exists which they have attributed as glycine–cysteine conjugate which can fragment from the protein during laser desorption. Similarly they have found Au_8 and Au_5 in MALDI TOF at pH 9. Wei *et al.* have first reported Au_{QCs}@Lyz but they did not show any mass spectrum for the clusters.[163] Chen *et al.* have reported blue emitting Au_8 clusters protected with Lyz at pH 3 and used the cluster for sensing glutathione in a single drop of blood.[162] They have shown MALDI MS of the clusters and proved that the cluster has a Au_8 core. They have proposed pH-dependent change in protein secondary structure that can lead to bigger clusters like Au_{25} at pH 12. Baksi *et al.* have reported the formation of Au_{10} core inside a single protein molecule of Lyz.[161] They have proved a single cluster within a single protein by careful examination of the protein aggregates. They have also shown through concentration-dependent study that a maximum of Au_{12} core is possible for a smaller protein like Lyz. They have also shown single cluster protected with multiple proteins at certain concentrations. We will discuss this in detail in the following subsection. There are several other protein protected clusters existing in the literature which were characterized by other tools but not by mass spectrometry.

Number of protein protected gold clusters is many compared to silver clusters due to inherent instability of silver clusters compared to gold clusters. Among them only a few have been characterized by MS. Mathew *et al.* have prepared Ag_{15} protected by BSA.[28] They have confirmed the core from multiple charge states of BSA (+2, +3 *etc.*) by calculating the mass difference from the parent BSA peak. The separation is about *m*/*z* 1.6 kDa for +1 charge state, whereas the mass difference is around 800 for +2 charge state and about 500 Da for +3 charge state. They have also studied the effect of $NaBH_4$ by varying the overall concentration of it and found that $NaBH_4$ helps in transforming Ag^+ to Ag^0 without changing the cluster core. In another report, Anand *et al.* have synthesized different Ag clusters protected with HSA.[154] They have found an Ag_9 core by the slow reduction of Ag^+ by HSA at pH 11 for 10 hours whereas Ag_{14} forms by rapid reduction of Ag^+ in presence of $NaBH_4$. Around 1 kDa mass shift was observed from the main BSA for Ag_9@HSA while the shift is about 1.5 kDa for Ag_{14}@HSA (see Fig. 12A).

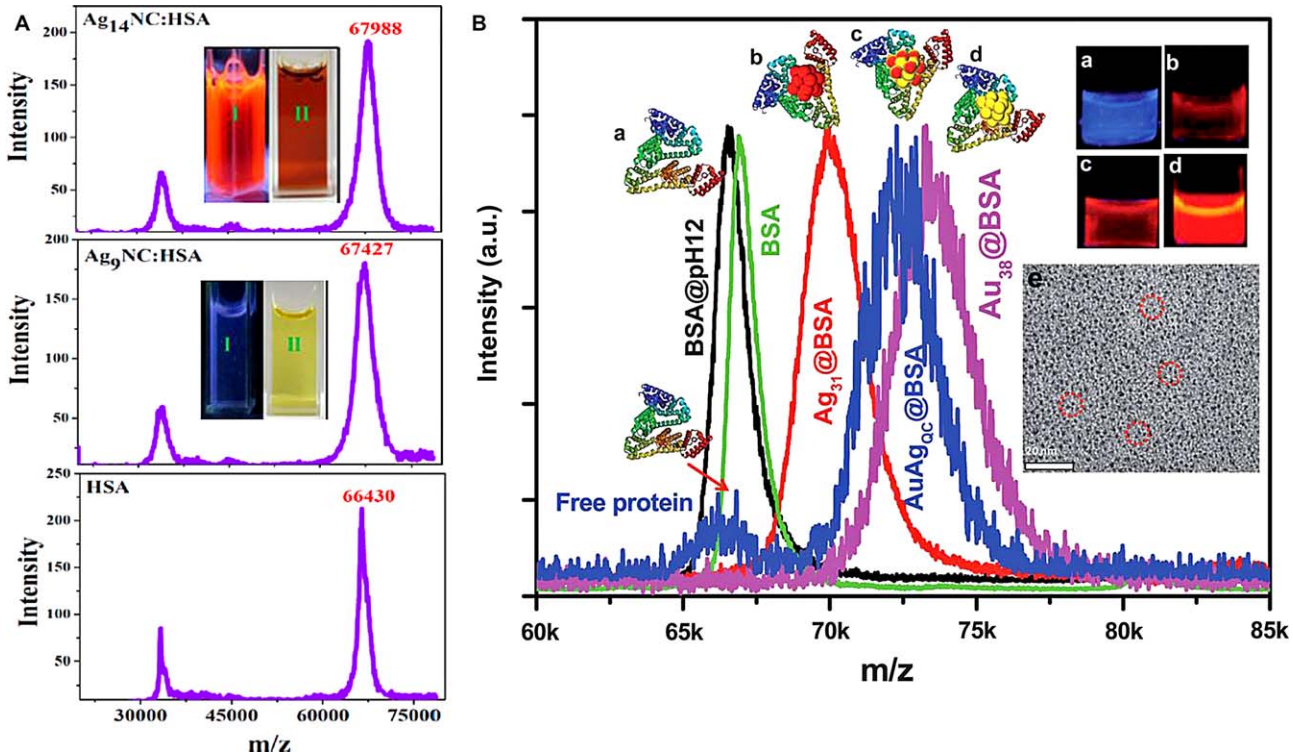

Fig. 12 (A) MALDI-TOF mass spectra of HSA (lower panel), Ag_9/HSA(middle panel), and Ag_{14}/HSA (upper panel). Corresponding photographs in visible as well as UV light are shown in the respective inset. Ag_9@HSA forms after 10 hours of reaction time at 37 °C at pH 11 without adding any external reducing agent. Ag_{14}@HSA can be prepared within a few minutes by adding $NaBH_4$ to a mixture of Ag^+, HSA at pH 11. Ag_{14} can be converted to Ag_9 simply by adding H_2O_2 in the solution within 5 minutes. On the other hand, Ag_9 can be converted to Ag_{14} by addition of $NaBH_4$. ©ACS Publishing. Reproduced with permission.[154] (B) MALDI MS showing alloy cluster formation from a 1 : 1 mixture of Au_{38}@BSA and Ag_{31}@BSA clusters. The alloy cluster can be assigned as $(AuAg)_{38}$@BSA. Schematic representations of all the species have been shown along with the corresponding peaks. Photographs of a) BSA at pH 12, b) Ag_{31}@BSA, c) $(AuAg)_{38}$@BSA and d) Au_{38}@BSA under UV light are shown in the inset. The as-formed alloy clusters have around 1 nm core size as shown in TEM image (inset e). Reproduced from Ref. 29 with permission from The Royal Society of Chemistry.

Gold and silver can form alloys in bulk as well as in the nano-regime. Gold-silver alloy clusters are reported for monolayer protected clusters. Mohanty *et al.* have reported Au@Ag quantum clusters using BSA as a protecting agent.[29] They have prepared Ag_{31}@BSA and Au_{38}@BSA and mixed them together in different proportions and found the formation of a tunable alloy cluster with intermediate mass (in between Ag_{31}@BSA and Au_{38}@BSA) (see Fig. 12B). For example, a 10 : 90 mixture of Ag_{31} : Au_{38} results in substitution of a few Au atoms by Ag while for the 90 : 10 mixture substitution of a few Ag atoms by gold occurs. Absence of both the parent cluster peaks suggests tuneable alloy cluster formation throughout the compositional window studied. They have also tried to prepare the alloy clusters by galvanic exchange assuming that in case Ag and Au clusters react with each other to form an alloy, there must be some reactivity of individual ions. They prepared Ag clusters and added $HAuCl_4$ in the solution and after reaction they observed the formation of AgCl confirming reactivity of the cluster and interchange of Ag atoms by Au. A similar kind of tuneable alloy clusters were observed in the case of Lyz also where different ratios of Au_{11}@Lyz and Ag_{13}@Lyz were mixed together.[177]

6.2 Non-noble metal clusters in protein templates

There are only a few reports of metal clusters other than gold and silver in the case of protein protected clusters. Goswami *et al.* have reported blue emitting copper clusters in BSA scaffold and used them as potential sensors for Pb^{2+}.[17] They have prepared blue emitting Cu clusters by mixing Cu salt with BSA at pH 12 at 55 °C. They have found two smaller cluster cores namely, Cu_5 and Cu_{13} in MALDI MS.

In another study they have made luminescent iron clusters in solution starting from hemoglobin (Hb), as the Fe source as well as protecting scaffold.[16] Pipiridine was used to bring Fe^{2+}/Fe^{3+} out from the porphyrin ring to the protein matrix and then subsequent reduction by $NaBH_4$ at room temperature to form yellow luminescent Fe clusters in solution. They have tried MALDI MS of the as-synthesized material to get an idea about the nuclearity. Hb showed two peaks in MALDI MS centered at *m*/*z* 15 230 due to α-globin chain and at *m*/*z* 15 990 due to β-globin chain. These two peaks shifted to *m*/*z* 15 760 and 16 500, respectively after cluster formation and the corresponding cluster core can be roughly assigned as Fe_{7-10}@Hb. This assignment might not be exactly correct due to the broadness of the peak and poor resolution at that mass range. ESI MS could be the best option to find the exact core in solution as it does not give much fragments like MALDI MS. They did not get any ESI MS of the as-synthesized Fe_{QCs}@Hb, which is a common problem for all protein protected clusters. To resolve this issue, they have tried ligand exchange with a smaller ligand known to form Fe nanoparticles, namely, trioctyl phosphineoxide (TOPO) as their ligand of choice and successfully extracted the exchanged product in chloroform. ESI MS of the ligand exchanged product using chloroform and acetonitrile as the solvent mixture showed multiple peaks due to Fe clusters namely, $[Fe_8(TOPO)(H_2O)_2]^+$, $[Fe_{10}(TOPO)_3(H_2O)_3]^+$, $[Fe_{12}(TOPO)_3(H_2O)_3]^+$ and $[Fe_{13}(TOPO)_2(H_2O)]^+$. Presence of H_2O was further confirmed by NMR.

Along with these major peaks, some small intensity peaks also appear which are mainly due to ligand and water attachments and detachments.

This was further proved using extensive MS/MS of the peaks. Most of the peaks show ligand loss in MS/MS. For example, $[Fe_{13}(TOPO)_2(H_2O)]^+$ and $[Fe_{10}(TOPO)_3(H_2O)_3]^+$ lose one TOPO to give $[Fe_{13}(TOPO)(H_2O)]^+$ and $[Fe_{10}(TOPO)_2(H_2O)_3]^+$, respectively in MS/MS. Another type of fragmentation was also observed when $[Fe_{12}(TOPO)_3(H_2O)_3]^+$ was subjected to MS/MS experiment. Two Fe losses were observed to give a final $[Fe_{10}(TOPO)_3(H_2O)_3]^+$ product. $[Fe_8(TOPO)(H_2O)_2]^+$ first loses one ligand to give $[Fe_8(H_2O)_2]^+$ and then two water molecules to give a bare Fe_8 core (see Fig. 13 for details).

There are some reports on other metal clusters like Pt but no mass spectrum was reported. Some of the protein and cluster systems along with their applications are listed in Table 2.

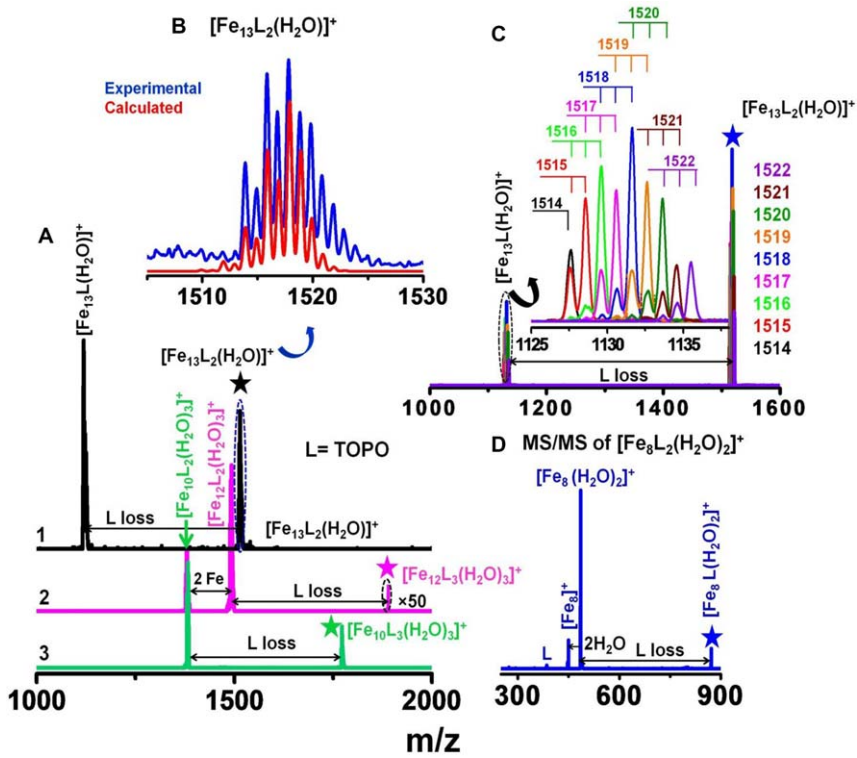

Fig. 13 (A) ESI MS/MS of 1) $[Fe_{13}(TOPO)_2(H_2O)]^+$, 2) $[Fe_{12}(TOPO)_3(H_2O)_3]^+$ and 3) $[Fe_{10}(TOPO)_3(H_2O)_3]^+$, showing subsequent ligand losses. For all cases parent ion is marked with * and for fragments compositions are indicated. $[Fe_{12}(TOPO)_3(H_2O)_3]^+$ shows different kind of fragmentations than $[Fe_{13}(TOPO)_2(H_2O)]^+$ and $[Fe_{10}(TOPO)_3(H_2O)_3]^+$. Here along with one ligand loss, two Fe loses was also observed. Intensity of $[Fe_{12}(TOPO)_3(H_2O)_3]^+$ was multiplied by 50 to make it visible. (B) $[Fe_{13}(TOPO)_2(H_2O)]^+$ spectrum is compared with the calculated spectrum. (C) MS/MS spectra of each peak in the $[Fe_{13}(TOPO)_2(H_2O)]^+$ envelope, with a mass width of 1 Da. Fragmented peaks (one ligand loss) are expanded in the inset showing isotope pattern mainly due to Fe. Isotope pattern of the parent ion is shown in B. (D) ESI MS/MS of $[Fe_8(TOPO)_2(H_2O)_2]^+$ showing ligand as well as water losses to give bare $[Fe_8]^+$ core. Reproduced from Ref. 16 with permission from The Royal Society of Chemistry.

Table 2 List of protein protected clusters and their applications.

Protein	Cluster	Application	Ref.
Bovine serum albumin	$Au_{4,13,25,20-25,16}$, Ag_{15} $Cu_{5,13}$, Au@Ag	Hg^{2+}, Cu^{2+}, Pb^{2+}, pyrophosphate, querectin, uric acid sensing, logic gate, bioimaging	17, 144–153, 170
Human serum albumin	Au, $Ag_{9,14}$	NOx sensing	155–157
Bovine lactoferrin	$Au_{13,25,34,40}$, Ag	Cluster evolution, FRET, conjugation with RGO, Cu^{2+} sensing, bio imaging	39, 154
Human serum transferrin	Au_{20-25}	Bio imaging, conjugation with RGO	177
Horse radish peroxidase	Au	H_2O_2 sensing	166
Pepsin	Au	Hg^{2+} sensing, blue, green and red emitting Au_{QC}	159
Hemoglobin	Fe	Luminescent iron cluster synthesis	16
Egg white	Au	H_2O_2 sensing	170
Egg shell membrane	Au, Ag	Solid platform synthesis, metal ion sensing	168
Human hair	Au	Solid platform synthesis, metal ion sensing	169
Insulin	$Au_{5,8,13}$	Bioactivity, Bio-imaging, cluster growth in crystals, solid state platform, tracking metabolism	167
Lysozyme	$Au_{8,\ 10-12}$, Ag_{13}. Au@Ag	Hg^{2+}, GSH sensing, cluster growth, deriving gas phase clusters	162–165
Trypsin	Au	Hg^{2+} sensing, bio-imaging	160
Chymotyipsin	Ag	Enzyme activity	161

6.3 Evolution of clusters

Chaudhari *et al.* have reported growth of Au clusters in Lf.[153] They have probed the experiment by varying the concentration of Lf and Au^{3+} and checked the change in MS with respect to time. In a typical synthesis, Au^{3+} was mixed with Lf to get a final concentration of 2.5 mM Au^{3+} and 150 μM of Lf in solution. Lf can interact with Au by various amino acids to form Au^{+}-Lf adduct. Lf in aqueous solution shows its molecular ion peak at *m*/*z* 83 kDa for the monomer and 166 kDa for the dimer formed by salt bridge interaction in solution. After Au adduct formation, the major peak at 83 kDa shifts to 86.2 kDa due to the attachment of 16 Au atoms to the protein. Reduction of Au^{3+} to Au^{+} by several amino acids was proved by XPS. When pH of the solution was elevated to 12.4 by means of NaOH addition, aromatic amino acids are capable of reducing Au^{+} to Au^{0}. As disulphide bonds between the cysteines (one of the major contributor of helical structure) break at this pH, free thiol group can bind to the Au and stabilize the as-formed clusters inside the protein. After 4 hours of NaOH addition, red luminescence starts appearing indicating the formation of the cluster core. At this stage, MALDI MS showed a clear peak at 86.7 kDa shifted by 22–23 gold atoms from the parent Lf peak. After 12 hours of incubation, they have observed a small hump at 85.6 kDa due to the appearance of Au_{13} along with

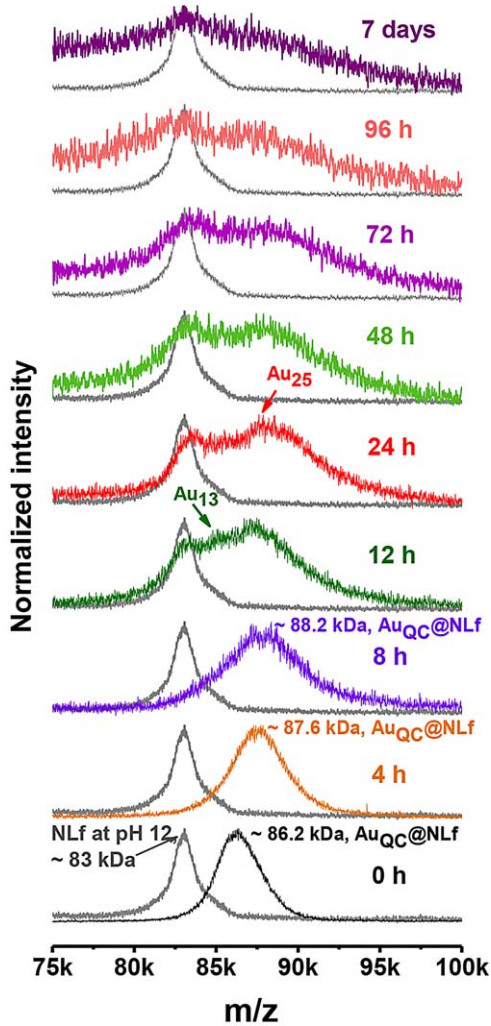

Fig. 14 Time dependent MALDI MS of Au_{QCs}@Lf showing evolution of Au_{25} cluster. Immediate addition of Au^{3+} to Lf results in Au^{+}-Lf adduct which is converted to the cluster core with incubation in basic conditions. Appearance of Au_{13} along with Au_{25} was observed after 12 hours of incubation. After 48 hours, only the Au_{25} core was observed without any further growth. ©ACS Publishing. Reproduced with permission.[153]

regeneration of free protein and formation of Au_{25} (see Fig. 14). This was explained in terms of intra and inter-protein reorganization of Au atoms due to aurophillic attraction of gold. When cluster core starts nucleating, it attracts other gold atoms from neighboring proteins which come out as free protein. To validate this hypothesis further,they have added Au^{3+} to the solution and saw that in this condition Au_{25} is forming with higher intensity and Au_{13} is absent suggesting complete conversion of all available gold to the Au_{25} core. This two-step approach is better than a single step method as the amount of cluster was increased, which is further supported by a two-fold increase in the luminescence intensity.

They have carried out similar kind of study with BSA also. They have noticed the formation of Au_{25} along with the Au_8 intermediate and concluded that the core might be the same but the growth depends completely on the nature of the protein. The above mentioned proteins are bigger (583 amino acid residues) and so it is expected that they can accommodate smaller 1 nm cluster core within. But when the protein size is smaller like insulin, there is a chance that clusters cannot form inside the protein rather multiple proteins can stabilize one core. Such type of studies were done with insulin where clusters were grown uniformly inside micro-crystals of protein and that was proved by depth dependent two-photon excitation spectroscopy and RAMAN spectroscopy but mass spectrum is not available for this specific system.[166]

Recently, Baksi *et al.* have reported growth of gold clusters inside a small protein Lyz (129 amino acid residues).[161] They have shown that a maximum of 12 atom gold core can be accommodated inside a single protein irrespective of the concentration of Au or protein used. Lyz forms aggregates both in solution and in gas phase. When clusters form, the main protein peak shifts by around m/z 2 kDa in the monomer region confirming the presence of Au_{10} core attached to the protein. There are shifts in the aggregate region also. They have seen peaks corresponding to Lyz^+, $Lyz_2{}^+$, $Lyz_3{}^+$ *etc.* for parent protein while, $(Au_{10}@Lyz)^+$, $(Au_{10}@Lyz)_2{}^+$, $(Au_{10}@Lyz)_3{}^+$, *etc.*, after cluster formation confirming similar kind of aggregation tendency of the protein after cluster formation. They have not seen any peak corresponding to $Au_{10}@Lyz_n$ which means that the cluster is inside the protein and while aggregating the whole species forms aggregates. Multiple proteins protecting a single cluster core was also observed when very low concentration of gold was used compared to the protein. In this case, amount of gold was not enough to saturate the protein and therefore when clusters started nucleating, multiple proteins could protect one single core. Therefore, it can be concluded that cluster core size is directly correlated to the protein size.

6.4 Gas phase clusters from protein templates

As discussed above, luminescent protein protected clusters exist in solution with zero valent oxidation state of the metal (for example, Au^0 state for Au clusters). Cluster forms *via* the metal bound protein complex (Au^+-Protein adduct for Au cluster formation) where metal is in its intermediate oxidation state.[153] In this section we will discuss a new class of materials which were observed recently by Baksi *et al.*[178] They have observed that when Au^+-Lyz adducts were subjected to laser ablation, some bare clusters were formed in the gas phase. When Au^{3+} was mixed with Lyz, Au was uptaken by the protein and a corresponding change is seen in the mass spectrum in the form of appearance of multiple peaks separated by m/z 197 due to Au attachments (Lyz^+ peak appears at m/z 14 300). Maximum 10 Au attachments were observed in the MALDI MS which was justified in terms of limited (eight cysteines forming 4 disulfide bonds) cysteine content. In the lower mass region (<10 kDa), multiple envelopes

can be observed consisting of multiple peaks separated by m/z 197 and the peak maxima of the envelopes were observed at $Au_{18}S_4^+$, Au_{25}^+ and Au_{38}^+. Au_{102}^+ was also observed but with less intensity (see Fig. 15A). Note that, Au_{25}, Au_{38} and Au_{102} are known to be magic number clusters when considered along with monolayer protection due to the shell closing electronic structure which have been crystallized already. Sulfur attachments were justified in terms of attachment of Au with the thiol group of cysteine residues. Au_{38} appears only at highest concentrations of Au^{3+}. In all other cases, in that region $(Au_n\text{-Lyz})^{2+}$ peaks appear with m/z 99 separation between the adjacent peak due to Au^{2+} (Au_{38}^+ mass is comparable with the $(Au_n\text{-Lyz})^{2+}$). They have also seen that Au_{38}^+ forms after a certain time of incubation of the adducts. Similar type of cluster formation was observed in negative ion mode also but the intensity was less compared to positive ion mode indicating that the clusters are more stable in the positive ion mode. To check whether these clusters form in solution or not, they have done ESI MS of the adducts and observed that maximum 3 Au attachment with the protein occurs which may be due to charge induced dissociation of large adducts at high charge state (+10, +11, *etc.*). There was no signature of bare clusters in the solution phase suggesting laser induced formation of such clusters in the gas phase. They have checked this phenomenon with other proteins namely, BSA and Lf also but Lyz was found to work best among these three. As already mentioned, Lyz is a small protein and can accommodate only up to 12 atom core inside it (see Section 5.3), it is obvious that the clusters (Au_{38} or Au_{102}) cannot form inside it. These clusters might be forming in the gas phase or may be forming in the solution itself and are loosely bound to the protein. Therefore, when they are subjected to laser ablation, they detach from the protein and appear as bare clusters.

When laser is fired, Au – bound protein adducts come to the gas phase. A gaseous plasma consisting of several ions, molecules, atoms and electrons is formed. A delay time is given before extraction of the ions which is enough for inter and intra molecular reaction in the plasma. Some of the Au atoms detach from the protein and they aggregate among themselves to form bare gas phase clusters. When these clusters nucleate from individual atoms, heat of aggregation should be removed from the system for stabilization. In this case, the above mentioned reactions are facilitated by the abundance of protein molecules and their gold adducts in the reaction zone, since their large mass slows down their movement and separation from the plasma cloud. Being a macromolecule, proteins have several degrees of freedom and can act as a heat bath. Several unimolecular reactions are possible like:

1. $Au_n + Au_m^+ \rightarrow Au_{n+m}^+ \quad n, m = 1, 2, 3, \ldots,$
2. $(\text{Lyz-Au}_n)^+ + Au_m \rightarrow (\text{Lyz-Au}_{n+m})^+ \quad n = 0, 1, 2, 3, \ldots; m = 1, 2, 3, \ldots,$
3. $(\text{Lyz-Au}_n)^+ + (\text{Lyz-Au}_m) \rightarrow (\text{Lyz-Au}_{n+k})^+ + (\text{Lyz-Au}_{m-k}) \quad n, m = 1, 2, 3, \ldots; k(<m) = 1, 2, 3, \ldots$

All these reactions are possible as the ions are extracted after a certain delay time (MALDI MS is generally performed by using a delayed extraction process) which is enough for aggregation reactions. By changing

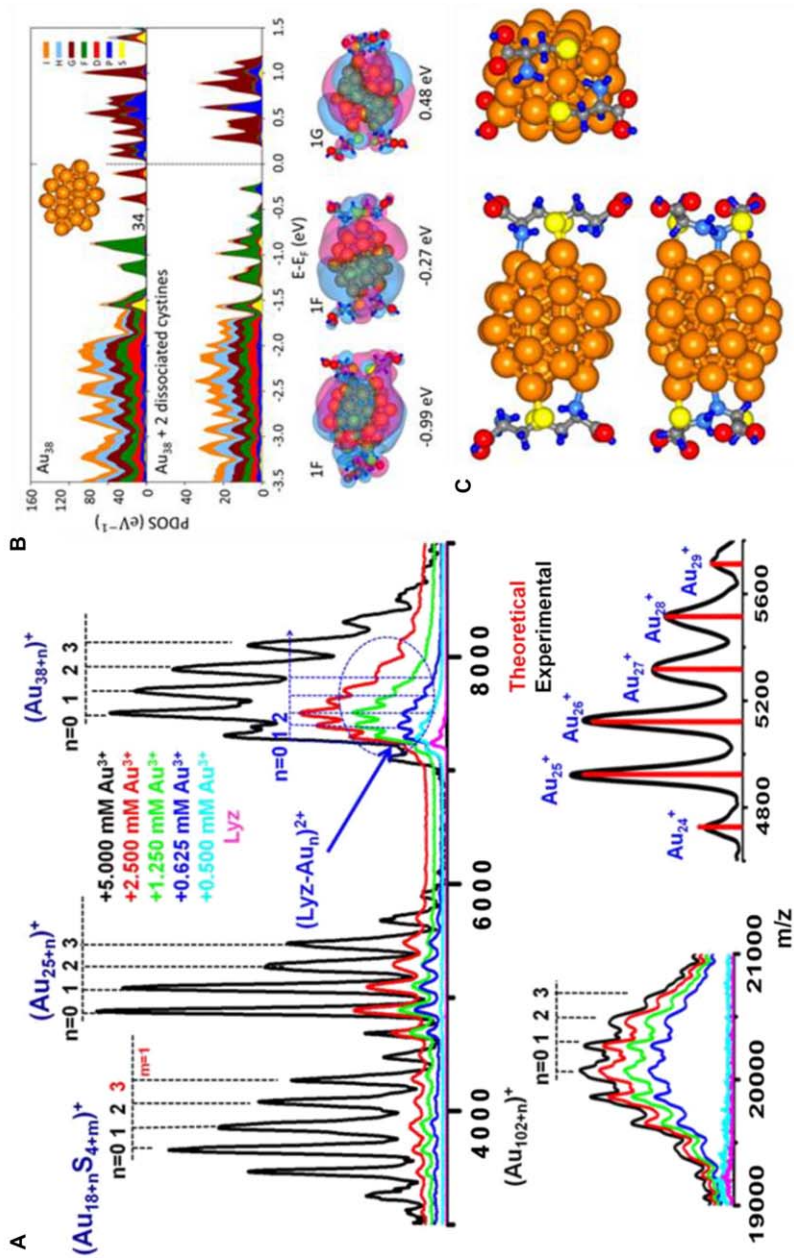

the delay time, one can get most stable product from mixture of possible products.

In proteins, cysteines form disulfide bond and exist as cystine units (dimer of cysteine) which is one of the causes of helicity of proteins. Keeping in mind the strong affinity of Au towards sulfur, it is assumed that Au ions bind to cysteine residues of the proteins. When Au ions are uptaken by the protein, disulfide bonds break and protein secondary structure is lost. This process can help the bare clusters to achieve their stability in gas phase. This was explained taking Au_{38} as a model through density functional theory calculations.

As mentioned above, Au_{25}, Au_{38} are known to be magic number clusters in the case of monolayer protection. But their gas phase analogues, bare Au_{25}, Au_{38} are not magic numbers by their electron count (magic numbers are 20, 34(40), 58, 92 *etc.*). For example, for Au_{38} to be a magic number, it must lose 4 electrons to get magic number stability which is possible only if interaction of protein with such clusters is considered. For lowering down the computational burden, they have considered only cystines, not the whole protein. If two cystines are bound to Au_{38} surface and dissociate to 4 cysteines, 4 electrons will be lost ($38 - 4 = 34$ e^-) and the cluster can get magic number stability. A distorted truncated octahedron (d-TO) structure was observed for bare Au_{38} which is different from its monolayer protected structure (see Fig. 15B). When a cystine binds to a d-TO Au_{38} surface, it does not change the overall structure or electronic arrangement. However, upon dissociation of two cystines to four cysteines, they adsorb strongly on the surface with a binding energy of 1.97 eV per cystine molecule (see Fig. 15C). Thus for dissociative binding of two cystines we get,

$$E[Au_{38}(d\text{-}TO)] + 2E[Cystine] - E[Au_{38}(Cysteine)_4] = 3.94\ eV$$

By this process, a HOMO–LUMO gap of 0.5 eV opens up and the cluster now has a magic number of electrons. The same calculation can be extended to Au_{102} where interaction with 5 cystines is required as the

Fig. 15 (A) MALDI MS of Au^+-Lyz in the linear positive mode showing formation of bare $Au_{18}S_4^+$, Au_{25}^+, Au_{38}^+ and Au_{102}^+. Three main envelopes were observed in the lower mass range (<10 kDa). Each envelope is composed of multiple peaks separated by *m*/*z* 197 due to Au. $Au_{18}S_4^+$, Au_{25}^+, Au_{38}^+ and Au_{102}^+ have the highest intensity compared to neighbouring peaks in the corresponding envelope indicating higher stability of these specific species in the gas phase compared to others. Au_{38} region overlaps with the +2 charge state of protein. Au_{38}^+ (and associated envelope) was observed at the highest concentration of Au^{3+} where peaks are separated by *m*/*z* 197 due to Au. This *m*/*z* 99 difference (between Au^{2+} and Au^+) can be easily resolved at the mass range. Experimental data matches well with the calculated value as shown for Au_{25}^+. (B) Calculated PDOS for Au_{38} showing distorted truncated octahedron structure whose energy is lower by 1.07 eV than that of an ideal TO structure. Dashed vertical line at $E-E_F = 0$ is showing the midpoint of HOMO and LUMO energy levels. In the lower panel PDOS of an optimized $Au_{38}(Cysteine)_4$ is shown. In the orbital isosurface images, positive and negative orbital values are coloured light blue and pink, and the orbital energies symmetries are marked. A stabilization energy (shell closure gap) of 0.5 eV was observed after interaction of Au_{38} cluster with two cystine residues of the protein, which ultimately got converted to four cysteines. (C) Three views of the structure of $Au_{38}(cyteine)_4$ with four adsorbed cysteine ($HO_2CCH(NH_2)CH_2S$-) residues, resulting from two dissociated cystine units.

nearest magic number is 92. This study clearly explains the interaction of protein with clusters in the gas phase.

In another study, they tried to dope foreign metals with these clusters in the gas phase.[177] Many transition metals like Ag, Cu, Pd, Pt, *etc.*, are known to form alloys both in bulk as well as in the nanoscale regime. They have used several metal ions covering 3d and 4d transition metals namely, Fe, Ni, Cr, Cu, Zn, Ag, Pd and Pt which are known to form alloys in bulk with gold. They have mixed Au^{+}-Lyz adduct and M-Lyz adduct in 3 : 1 ratio (optimized from several concentration dependent studies) and found that only Pd was recognized in the gas phase by gold and formed an alloy. Other metal ions act as catalyst for specific Au cluster formation. For example, Ni^{2+}, Cr^{3+} and Fe^{2+} enhance the intensity of Au_{25}^{+} but does not form any alloy with gold in gas phase. In presence of Pt, the $Au_{18}S_4$ region was enhanced and all the other peak positions remained almost the same. As molecular weights of Au (197) and Pt (195) are nearly the same, it is not possible to conclude whether any alloy was formed or not. Solely Au_{25}^{+} was formed when Cu^{2+} was added to the system, possibly due to substitution of Au binding sites by Cu which was reflected in the total number of Au attachments to the protein. Although Ag is most well-known to form alloy with gold in all solutions (bulk, nanoparticles, monolayer and protein protected clusters) but such an alloy was not detected in the gas phase. In the case of Pd, maximum of two Pd attachments were observed in the gas phase. Total shape of the envelope changed after alloy formation. Maximum peak was observed for $Au_{20}Pd_2S^{+}$ (comparable to Au_{25}^{+} in electron count). Although $Au_{24}Pd$ is the most stable species in solution state but in gas phase $Au_{27}Pd^{+}$ showed the maximum intensity although the neighboring peaks do not vary much in terms of abundance. No alloy formation was observed in the Au_{38} region and the relative intensity (Au_{25} to Au_{38}) is higher here compared to pure gold-adducts. This signifies catalytic enhancement of stability of Au_{38} in presence of Pd. This was further confirmed when the mixed adducts (Au-Lyz and Pd-Lyz) were incubated for two days and then subjected to laser ablation, Au_{38} appeared as the most intense peak (more intense than the main protein peak). Another envelope appears after the Au_{38} region which was originally absent only in the case of Au. In this region, $Au_{47}PdS_2^{+}$ was the most intense one although it is not a magic number implying that Pd facilitates formation of metastable clusters in the gas phase. Alloy formation occurs in the gas phase irrespective of the physical mixture of Au and Pd adducts or direct addition of Pd^{2+} salt into Au adduct solution implying simultaneous Pd uptake by the protein in presence of Au which was proven further by ESI MS.

7 Conclusion and future perspectives

Investigation of atomically precise pieces of matter by mass spectrometry has given information on several new cluster systems. Their chemistry and materials science have advanced tremendously in the past few years. Each of those investigations has used mass spectrometry extensively. Tandem mass spectrometry of several clusters and cluster fragments

must be investigated to know them in detail. Some of those gas phase products can only be investigated with the help of mass spectrometry. While excellent mass spectra have become possible due to new developments in mass spectrometry, some of those studies have not been possible on a few other clusters, such as MALDI MS of $Ag_{44}SR_{30}^{4-}$. New methods for MALDI have to be found for such systems. ESI MS has not been possible so far on protein protected clusters. It is also important to note that studies on clusters have given several challenges, especially in the isolation of isomeric clusters. As cluster systems become more complex, ion mobility may become one of the important aspects of mass analysis of clusters. Chemistry of cluster ions in the gas phase, derived from clusters in solution will become attractive. There is also a possibility to study the properties of naked clusters derived from protein templates, especially their catalysis. All these studies will make this area rich in the coming years.

Acknowledgements

We thank the contributions of our co-workers who have contributed to the original research reported in this chapter. We thank the Nano Mission, Government of India, for generously supporting our research. We are also grateful to the Department of Science and Technology for sponsoring several research grants which made some of these studies possible.

References

1 J. B. Fenn, M. Mann, C. K. Meng, S. F. Wong and C. M. Whitehouse, *Mass Spectrom. Rev.*, 1990, **9**, 37.
2 D. J. Harvey, *Mass Spectrom. Rev.*, 1999, **18**, 349.
3 R. Aebersold and M. Mann, *Nature*, 2003, **422**, 198.
4 K. Dettmer, P. A. Aronov and B. D. Hammock, *Mass Spectrom. Rev.*, 2007, **26**, 51.
5 L. G. Abdul Halim, S. Ashraf, K. Katsiev, A. R. Kirmani, N. Kothalawala, D. H. Anjum, S. Abbas, A. Amassian, F. Stellacci, A. Dass, I. Hussain and O. M. Bakr, *J. Mater. Chem. A*, 2013, **1**, 10148.
6 L. A. Angel, L. T. Majors, A. C. Dharmaratne and A. Dass, *ACS Nano*, 2010, **4**, 4691.
7 T. M. Bernhardt, *Int. J. Mass Spectrom.*, 2005, **243**, 1.
8 I. Chakraborty, R. G. Bhuin, S. Bhat and T. Pradeep, *Nanoscale*, 2014, **6**, 8561.
9 A. Dass, A. Stevenson, G. R. Dubay, J. B. Tracy and R. W. Murray, *J. Am. Chem. Soc.*, 2008, **130**, 5940.
10 A. C. Dharmaratne, T. Krick and A. Dass, *J. Am. Chem. Soc.*, 2009, **131**, 13604.
11 B. Domon and R. Aebersold, *Science*, 2006, **312**, 212.
12 C. A. Fields-Zinna, M. C. Crowe, A. Dass, J. E. Weaver and R. W. Murray, *Langmuir*, 2009, **25**, 7704.
13 C. A. Fields-Zinna, M. C. Crowe, A. Dass, J. E. F. Weaver and R. W. Murray, *Langmuir*, 2009, **25**, 7704.

14 C. A. Fields-Zinna, J. S. Sampson, M. C. Crowe, J. B. Tracy, J. F. Parker, A. M. deNey, D. C. Muddiman and R. W. Murray, *J. Am. Chem. Soc.*, 2009, **131**, 13844.
15 A. Ghosh, T. Udayabhaskararao and T. Pradeep, *J. Phys. Chem. Lett.*, 2012, **3**, 1997.
16 N. Goswami, A. Baksi, A. Giri, P. L. Xavier, G. Basu, T. Pradeep and S. K. Pal, *Nanoscale*, 2013, **6**, 1848.
17 N. Goswami, A. Giri, M. S. Bootharaju, P. L. Xavier, T. Pradeep and S. K. Pal, *Anal. Chem.*, 2011, **83**, 9676.
18 J. Guo, S. Kumar, M. Bolan, A. Desireddy, T. P. Bigioni and W. P. Griffith, *Anal. Chem.*, 2012, **84**, 5304.
19 K. M. Harkness, D. E. Cliffel and J. A. McLean, *Analyst*, 2010, **135**, 868.
20 K. M. Harkness, L. S. Fenn, D. E. Cliffel and J. A. McLean, *Anal. Chem.*, 2010, **82**, 3061.
21 K. M. Harkness, B. C. Hixson, L. S. Fenn, B. N. Turner, A. C. Rape, C. A. Simpson, B. J. Huffman, T. C. Okoli, J. A. McLean and D. E. Cliffel, *Anal. Chem.*, 2010, **82**, 9268.
22 K. M. Harkness, Y. Tang, A. Dass, J. Pan, N. Kothalawala, V. J. Reddy, D. E. Cliffel, B. Demeler, F. Stellacci, O. M. Bakr and J. A. McLean, *Nanoscale*, 2012, **4**, 4269.
23 I. Katakuse, T. Ichihara, Y. Fujita, T. Matsuo, T. Sakurai and H. Matsuda, *Int. J. Mass Spectrom. Ion Processes*, 1985, **67**, 229.
24 I. Katakuse, T. Ichihara, Y. Fujita, T. Matsuo, T. Sakurai and H. Matsuda, *Int. J. Mass Spectrom. Ion Processes*, 1986, **74**, 33.
25 C. Kumara and A. Dass, *Nanoscale*, 2011, **3**, 3064.
26 C. Kumara and A. Dass, *Nanoscale*, 2012, **4**, 4084.
27 X. Li, *Cluster Anions in the Gas Phase: Time-of-flight Mass Spectrometry and Photoelectron Spectroscopic Studies*, Thesis, Johns Hopkins University, 2009.
28 A. Mathew, P. R. Sajanlal and T. Pradeep, *J. Mater. Chem.*, 2010, **21**, 11205.
29 J. S. Mohanty, P. L. Xavier, K. Chaudhari, M. S. Bootharaju, N. Goswami, S. K. Pal and T. Pradeep, *Nanoscale*, 2012, **4**, 4255.
30 R. J. O'Hair and G. Khairallah, *J. Cluster Sci.*, 2004, **15**, 331.
31 H. Qian, Y. Zhu and R. Jin, *Proc. Natl. Acad. Sci.*, 2012, **109**, 696.
32 K. Salorinne, X. Chen, R. W. Troff, M. Nissinen and H. Hakkinen, *Nanoscale*, 2012, **4**, 4095.
33 D. M. D. J. Singh, T. Pradeep, J. Bhattacharjee and U. V. Waghmare, *J. Am. Soc. Mass Spectrom*, 2007, **18**, 2191.
34 Z. Takats, J. M. Wiseman, B. Gologan and R. G. Cooks, *Science*, 2004, **306**, 471.
35 J. B. Tracy, G. Kalyuzhny, M. C. Crowe, R. Balasubramanian, J.-P. Choi and R. W. Murray, *J. Am. Chem. Soc.*, 2007, **129**, 6706.
36 T. Udayabhaskararao, M. S. Bootharaju and T. Pradeep, *Nanoscale*, 2013, **5**, 9404.
37 G. Wang and R. B. Cole, *Anal. Chem.*, 1998, **70**, 873.
38 Z. Wu, E. Lanni, W. Chen, M. E. Bier, D. Ly and R. Jin, *J. Am. Chem. Soc.*, 2009, **131**, 16672.
39 P. L. Xavier, K. Chaudhari, P. K. Verma, S. K. Pal and T. Pradeep, *Nanoscale*, 2010, **2**, 2769.
40 I. Chakraborty, J. Erusappan, A. Govindarajan, S. K. Sugi, U. B. R. Thumu, A. Ghosh and T. Pradeep, *Nanoscale*, 2014.
41 I. Chakraborty, A. Govindarajan, J. Erusappan, A. Ghosh, T. Pradeep, B. Yoon, R. L. Whetten and U. Landman, *Nano Lett.*, 2012, **12**, 5861.

42 I. Chakraborty, W. Kurashige, K. Kanehira, L. Gell, H. Häkkinen, Y. Negishi and T. Pradeep, *J. Phys. Chem. Lett.*, 2013, 3351.
43 A. Dass, *J. Am. Chem. Soc.*, 2009, **131**, 11666.
44 A. Dass, *J. Am. Chem. Soc.*, 2011, **133**, 19259.
45 A. Ganguly, I. Chakraborty, T. Udayabhaskararao and T. Pradeep, *J. Nanopart. Res.*, 2013, **15**, 1.
46 Y. Negishi, W. Kurashige, Y. Niihori, T. Iwasa and K. Nobusada, *Phys. Chem. Chem. Phys.*, 2010, **12**, 6219.
47 Y. Negishi, K. Nobusada and T. Tsukuda, *J. Am. Chem. Soc.*, 2005, **127**, 5261.
48 Y. Niihori, M. Matsuzaki, T. Pradeep and Y. Negishi, *J. Am. Chem. Soc.*, 2013, **135**, 4946.
49 M. Moskovits, *Annu. Rev. Phys. Chem.*, 1991, **42**, 465.
50 W. A. de Heer, *Rev. Mod. Phys.*, 1993, **65**, 611.
51 M. D. Morse, *Chem. Rev.*, 1986, **86**, 1049.
52 T. Pradeep, *Nano: The Essentials Understanding Nanoscience and Nanotechnology*, Tata McGraw-Hill Education, 2007.
53 W. D. Knight, K. Clemenger, W. A. de Heer, W. A. Saunders, M. Y. Chou and M. L. Cohen, *Phys. Rev. Lett.*, 1984, **52**, 2141.
54 D. H. E. Gross and M. E. Madjet, *Z. Phys. B: Condens. Matter*, 1997, **104**, 541.
55 H. Rashidzadeh and B. Guo, *Chem. Phys. Lett.*, 1999, **310**, 466.
56 H. W. Kroto, J. R. Heath, S. C. O'Brien, R. F. Curl and R. E. Smalley, *Nature*, 1985, **318**, 162.
57 S. Maruyama, M. Kohno and S. Inque, *Therm. Sci. Eng.*, 1999, **7**, 1.
58 D. M. D. J. Singh, T. Pradeep, J. Bhattacharjee and U. V. Waghmare, *J. Phys. Chem. A*, 2005, **109**, 7339.
59 T. Lange and T. P. Martin, *Angew. Chem., Int. Ed. Engl.*, 1992, **31**, 172.
60 J. T. Lyon, P. Gruene, A. Fielicke, G. Meijer, E. Janssens, P. Claes and P. Lievens, *J. Am. Chem. Soc.*, 2009, **131**, 1115.
61 J. F. Gal, R. Grover, P. C. Maria, L. Operti, R. Rabezzana, G. A. Vaglio and P. Volpe, *J. Phys. Chem.*, 1994, **98**, 11978.
62 M. Haertelt, J. T. Lyon, P. Claes, J. de Haeck, P. Lievens and A. Fielicke, *J. Chem. Phys.*, 2012, 136.
63 J. Sun, H.-F. Gruetzmacher and C. Lifshitz, *J. Phys. Chem.*, 1994, **98**, 4536.
64 P. P. Radi, T. L. Bunn, P. R. Kemper, M. E. Molchan and M. T. Bowers, *J. Chem. Phys.*, 1988, **88**, 2809.
65 A. A. Shvartsburg, B. Liu, Z.-Y. Lu, C.-Z. Wang, M. F. Jarrold and K.-M. Ho, *Phys. Rev. Lett.*, 1999, **83**, 2167.
66 A. N. Alexandrova, A. I. Boldyrev, H.-J. Zhai and L.-S. Wang, *Coord. Chem. Rev.*, 2006, **250**, 2811.
67 M. Krempp, R. Damrauer, C. H. DePuy and Y. Keheyan, *J. Am. Chem. Soc.*, 1994, **116**, 3629.
68 K. Larsson, *J. Phys. IV*, 2001, **11**(Pr3), 423.
69 J. M. L. Martin and P. R. Taylor, *J. Phys. Chem. A*, 1998, **102**, 2995.
70 H.-J. Zhai, Q. Chen, H. Bai, S.-D. Li and L.-S. Wang, *Acc. Chem. Res.*, 2014, **47**, 2435–2445.
71 A. Muller and C. Serain, *Acc. Chem. Res.*, 2000, **33**, 2.
72 R. Tenne and C. N. R. Rao, *Philos. Trans. R. Soc., A*, 2004, **362**, 2099.
73 R. Tenne, M. Homyonfer and Y. Feldman, *Chem. Mater.*, 1998, **10**, 3225.
74 R. Tenne, M. Homyonfer and Y. Feldman, *Adv. Met. Semicond. Clusters*, 1998, **4**, 227.
75 R. Tenne and M. Redlich, *Chem. Soc. Rev.*, 2010, **39**, 1423.

76 M. Bar-Sadan and R. Tenne, *Inorganic Nanoparticles: Synthesis, Applications and Perspectives*, CRC Press, 2011, p. 441.
77 O. Brontvein, D. G. Stroppa, R. Popovitz-Biro, A. Albu-Yaron, M. Levy, D. Feuerman, L. Houben, R. Tenne and J. M. Gordon, *J. Am. Chem. Soc.*, 2012, **134**, 16379.
78 S. Y. Hong, R. Kreizman, R. Rosentsveig, A. Zak, J. Sloan, A. N. Enyashin, G. Seifert, M. L. H. Green and R. Tenne, *Eur. J. Inorg. Chem.*, 2010, 4233.
79 R. Kreizman, S. Y. Hong, F. L. Deepak, A. N. Enyashin, R. Popovitz-Biro, A. Albu-Yaron, G. Seifert and R. Tenne, *Routes for Core-shell Inorganic Nanotubes*, American Chemical Society, 2010, p. FUEL.
80 R. Kreizman, S. Y. Hong, J. Sloan, R. Popovitz-Biro, A. Albu-Yaron, G. Tobias, B. Ballesteros, B. G. Davis, M. L. H. Green and R. Tenne, *Angew. Chem., Int. Ed.*, 2009, **48**, 1230.
81 R. Levi, O. Bitton, G. Leitus, R. Tenne and E. Joselevich, *Nano Lett.*, 2013, **13**, 3736.
82 R. Tenne, *Angew. Chem., Int. Ed.*, 2003, **42**, 5124.
83 R. Tenne and M. Bar-Sadan, *Isr. J. Chem.*, 2010, **50**, 393.
84 *Inorganic Nanotubes and Nanostructures*, ed. R. Tenne and M. Bar-Sadan, [In: *Isr. J. Chem.*, 2010; **50**(4)], Wiley-VCH Verlag GmbH & Co. KGaA, 2010.
85 A. Voldman, D. Zbaida, H. Cohen, G. Leitus and R. Tenne, *Macromol. Chem. Phys.*, 2013, **214**, 2007.
86 X. Wang, Y. Xie and Q. Guo, *Chem. Commun.*, 2003, 2688.
87 F. Diederich, *Nature*, 1994, **369**, 199.
88 Y. R. Hacohen, E. Grunbaum, R. Tenne, J. Sloan and J. L. Hutchison, *Nature*, 1998, **395**, 336.
89 M. Brust, M. Walker, D. Bethell, D. J. Schiffrin and R. Whyman, *J. Chem. Soc., Chem. Commun.*, 1994, 801.
90 M. Heaven, A. Dass, P. White, K. Holt and R. Murray, *J. Am. Chem. Soc.*, 2008, **130**, 3754.
91 M. J. Hostetler, J. E. Wingate, C.-J. Zhong, J. E. Harris, R. W. Vachet, M. R. Clark, J. D. Londono, S. J. Green, J. J. Stokes, G. D. Wignall, G. L. Glish, M. D. Porter, N. D. Evans and R. W. Murray, *Langmuir*, 1998, **14**, 17.
92 R. S. Ingram, M. J. Hostetler and R. W. Murray, *J. Am. Chem. Soc.*, 1997, **119**, 9175.
93 R. S. Ingram, M. J. Hostetler, R. W. Murray, T. G. Schaaff, J. T. Khoury, R. L. Whetten, T. P. Bigioni, D. K. Guthrie and P. N. First, *J. Am. Chem. Soc.*, 1997, **119**, 9279.
94 V. L. Jimenez, D. G. Georganopoulou, R. J. White, A. S. Harper, A. J. Mills, D. Lee and R. W. Murray, *Langmuir*, 2004, **20**, 6864.
95 R. L. Wolfe, R. Balasubramanian, J. B. Tracy and R. W. Murray, *Langmuir*, 2006, **23**, 2247.
96 I. Chakraborty, T. Udayabhaskararao and T. Pradeep, *Chem. Commun.*, 2012, **48**, 6788.
97 K. S. Sugi, I. Chakraborty, T. Udayabhaskararao, J. S. Mohanty and T. Pradeep, *Part. Part. Syst. Charact.*, 2013, **30**, 241–243.
98 R. L. Whetten, J. T. Khoury, M. M. Alvarez, S. Murthy, I. Vezmar, Z. L. Wang, P. W. Stephens, C. L. Cleveland, W. D. Luedtke and U. Landman, *Adv. Mater.*, 1996, **8**, 428.
99 T. G. Schaaff, G. Knight, M. N. Shafigullin, R. F. Borkman and R. L. Whetten, *J. Phys. Chem. B*, 1998, **102**, 10643.
100 M. Zhu, C. M. Aikens, F. J. Hollander, G. C. Schatz and R. Jin, *J. Am. Chem. Soc.*, 2008, **130**, 5883.
101 H. Häkkinen, M. Walter and H. Grönbeck, *J. Phys. Chem. B*, 2006, **110**, 9927.

102 A. Das, T. Li, K. Nobusada, C. Zeng, N. L. Rosi and R. Jin, *J. Am. Chem. Soc.*, 2013, **135**, 18264.
103 C. Zeng, T. Li, A. Das, N. L. Rosi and R. Jin, *J. Am. Chem. Soc.*, 2013, **135**, 10011.
104 C. Zeng, H. Qian, T. Li, G. Li, N. L. Rosi, B. Yoon, R. N. Barnett, R. L. Whetten, U. Landman and R. Jin, *Angew. Chem., Int. Ed.*, 2012, **51**, 13114–13118.
105 H. Qian, W. T. Eckenhoff, Y. Zhu, T. Pintauer and R. Jin, *J. Am. Chem. Soc.*, 2010, **132**, 8280.
106 P. D. Jadzinsky, G. Calero, C. J. Ackerson, D. A. Bushnell and R. D. Kornberg, *Science*, 2007, **318**, 430.
107 H. Yang, J. Lei, B. Wu, Y. Wang, M. Zhou, A. Xia, L. Zheng and N. Zheng, *Chem. Commun.*, 2012, **49**, 300.
108 H. Yang, Y. Wang and N. Zheng, *Nanoscale*, 2013, **5**, 2674.
109 A. Desireddy, B. E. Conn, J. Guo, B. Yoon, R. N. Barnett, B. M. Monahan, K. Kirschbaum, W. P. Griffith, R. L. Whetten, U. Landman and T. P. Bigioni, *Nature*, 2013, **501**, 399.
110 H. Yang, Y. Wang, H. Huang, L. Gell, L. Lehtovaara, S. Malola, H. Hakkinen and N. Zheng, *Nat. Commun.*, 2013, **4**, 2422.
111 H. Qian, W. T. Eckenhoff, Y. Zhu, T. Pintauer and R. Jin, *J. Am. Chem. Soc.*, 2012, **132**, 8280.
112 Y. Negishi, N. K. Chaki, Y. Shichibu, R. L. Whetten and T. Tsukuda, *J. Am. Chem. Soc.*, 2007, **129**, 11322.
113 T. U. B. Rao and T. Pradeep, *Angew. Chem., Int. Ed.*, 2010, **49**, 3925.
114 T. U. B. Rao, B. Nataraju and T. Pradeep, *J. Am. Chem. Soc.*, 2010, **132**, 16304.
115 I. Chakraborty, W. Kurashige, K. Kanehira, L. Gell, H. Hakkinen, Y. Negishi and T. Pradeep, *J. Phys. Chem. Lett.*, 2013, **4**, 3351.
116 S. Giuffrida, G. Ventimiglia, F. L. Callari and S. Sortino, *Eur. J. Inorg. Chem.*, 2006, **2006**, 4022.
117 X. Yuan, Z. Luo, Q. Zhang, X. Zhang, Y. Zheng, J. Y. Lee and J. Xie, *ACS Nano*, 2011, **5**, 8800.
118 X. Huang, B. Li, L. Li, H. Zhang, I. Majeed, I. Hussain and B. Tan, *J. Phys. Chem. C*, 2011, **116**, 448.
119 X. Le Guével, V. Trouillet, C. Spies, G. Jung and M. Schneider, *J. Phys. Chem. C*, 2012, **116**, 6047.
120 H. Kawasaki, H. Yamamoto, H. Fujimori, R. Arakawa, M. Inada and Y. Iwasaki, *Chem. Commun.*, 2010, **46**, 3759.
121 C. K. Yee, R. Jordan, A. Ulman, H. White, A. King, M. Rafailovich and J. Sokolov, *Langmuir*, 1999, **15**, 3486.
122 S. Chen, K. Huang and J. A. Stearns, *Chem. Mater.*, 2000, **12**, 540.
123 F. P. Zamborini, S. M. Gross and R. W. Murray, *Langmuir*, 2000, **17**, 481.
124 I. Quiros, M. Yamada, K. Kubo, J. Mizutani, M. Kurihara and H. Nishihara, *Langmuir*, 2002, **18**, 1413.
125 J. E. Martin, J. P. Wilcoxon, J. Odinek and P. Provencio, *J. Phys. Chem. B*, 2002, **106**, 971.
126 Y. Negishi, H. Murayama and T. Tsukuda, *Chem. Phys. Lett.*, 2002, **366**, 561.
127 W. Wei, Y. Lu, W. Chen and S. Chen, *J. Am. Chem. Soc.*, 2011, **133**, 2060.
128 R. S. Dhayal, J.-H. Liao, Y.-R. Lin, P.-K. Liao, S. Kahlal, J.-Y. Saillard and C. W. Liu, *J. Am. Chem. Soc.*, 2013, **135**, 4704.
129 Y. Negishi, K. Igarashi, K. Munakata, W. Ohgake and K. Nobusada, *Chem. Commun.*, 2012, **48**, 660.
130 Y. Negishi, T. Iwai and M. Ide, *Chem. Commun.*, 2010, **46**, 4713.

131 Y. Negishi, K. Munakata, W. Ohgake and K. Nobusada, *J. Phys. Chem. Lett.*, 2012, **3**, 2209.
132 H. Qian, D.-e. Jiang, G. Li, C. Gayathri, A. Das, R. R. Gil and R. Jin, *J. Am. Chem. Soc.*, 2012, **134**, 16159.
133 S. R. Biltek, S. Mandal, A. Sen, A. C. Reber, A. F. Pedicini and S. N. Khanna, *J. Am. Chem. Soc.*, 2012, **135**, 26.
134 R. Ferrando, J. Jellinek and R. L. Johnston, *Chem. Rev.*, 2008, **108**, 845.
135 T. Udayabhaskararao, Y. Sun, N. Goswami, S. K. Pal, K. Balasubramanian and T. Pradeep, *Angew. Chem., Int. Ed.*, 2012, **51**, 2155.
136 V. R. Jupally and A. Dass, *Phys. Chem. Chem. Phys.*, 2014, **16**, 10473.
137 W. Kurashige, K. Munakata, K. Nobusada and Y. Negishi, *Chem. Commun.*, 2013, **49**, 5447.
138 S. L. Christensen, M. A. MacDonald, A. Chatt, P. Zhang, H. Qian and R. Jin, *J. Phys. Chem. C*, 2012, **116**, 26932.
139 P. L. Xavier, K. Chaudhari, A. Baksi and T. Pradeep, *Nano Rev.*, 2012, **3**, 14767and the references cited there in.
140 Y. Wang, Y. Cui, Y. Zhao, R. Liu, Z. Sun, W. Li and X. Gao, *Chem. Commun.*, 2012, **48**, 871.
141 J. T. Petty, J. Zheng, N. V. Hud and R. M. Dickson, *J. Am. Chem. Soc.*, 2004, **126**, 5207.
142 J. Zheng, C. Zhang and R. M. Dickson, *Phys. Rev. Lett.*, 2004, **93**, 1.
143 J.-m. Liu, M.-l. Cui, S.-L. Jiang, X.-x. Wang, L.-p. Lin, L. Jiao, L.-H. Zhang and Z.-Y. Zheng, *Anal. Methods*, 2013, **5**, 3942–3947.
144 X. Wen, P. Yu, Y.-R. Toh, A.-C. Hsu, Y.-C. Lee and J. Tang, *J. Phys. Chem. C*, 2012, **116**, 19032.
145 H.-W. Li, K. Ai and Y. Wu, *Chem. Commun.*, 2011, **47**, 9852.
146 X. Le Guével, B. Hötzer, G. Jung, K. Hollemeyer, V. Trouillet and M. Schneider, *J. Phys. Chem. C*, 2011, **115**, 10955.
147 J. Xie, Y. Zheng and J. Y. Ying, *Chem. Commun.*, 2010, **46**, 961.
148 M. A. Habeeb Muhammed, P. K. Verma, S. K. Pal, A. Retnakumari, M. Koyakutty, S. Nair and T. Pradeep, *Chem. – Eur. J.*, 2010, **16**, 10103.
149 Y. Yue, T.-Y. Liu, H.-W. Li, Z. Liu and Y. Wu, *Nanoscale*, 2012, **4**, 2251.
150 J. Xie, Y. Zheng and J. Y. Ying, *J. Am. Chem. Soc.*, 2009, **131**, 888.
151 P.-C. Chen, C.-K. Chiang and H.-T. Chang, *J. Nanopart. Res.*, 2012, **15**, 1.
152 Y. Yu, Z. Luo, C. S. Teo, Y. N. Tan and J. Xie, *Chem. Commun.*, 2013, **49**, 9740.
153 K. Chaudhari, P. L. Xavier and T. Pradeep, *ACS Nano*, 2011, **5**, 8816.
154 U. Anand, S. Ghosh and S. Mukherjee, *J. Phys. Chem. Lett.*, 2012, **3**, 3605.
155 L. Yan, Y. Cai, B. Zheng, H. Yuan, Y. Guo, D. Xiao and M. M. F. Choi, *J. Mater. Chem.*, 2012, **22**, 1000.
156 P.-H. Chan and Y.-C. Chen, *Anal. Chem.*, 2012, **84**, 8952.
157 S. M. Lystvet, S. Volden, G. Singh, I. M. Rundgren, H. Wen, Ø. Halskau and W. R. Glomm, *J. Phys. Chem. C*, 2013, **117**, 2230.
158 H. Kawasaki, K. Hamaguchi, I. Osaka and R. Arakawa, *Adv. Funct. Mater.*, 2011, **21**, 3508.
159 H. Kawasaki, K. Yoshimura, K. Hamaguchi and R. Arakawa, *Anal. Sci.*, 2011, **27**, 591.
160 S. S. Narayanan and S. K. Pal, *J. Phys. Chem. C*, 2008, **112**, 4874.
161 A. Baksi, P. L. Xavier, K. Chaudhari, N. Goswami, S. K. Pal and T. Pradeep, *Nanoscale*, 2013, **5**, 2009.
162 T.-H. Chen and W.-L. Tseng, *Small*, 2012, **8**, 1912.
163 H. Wei, Z. Wang, L. Yang, S. Tian, C. Hou and Y. Lu, *Analyst*, 2010, **135**, 1406.

164 T. Zhou, Y. Huang, W. Li, Z. Cai, F. Luo, C. J. Yang and X. Chen, *Nanoscale*, 2012, **4**, 5312.
165 F. Wen, Y. Dong, L. Feng, S. Wang, S. Zhang and X. Zhang, *Anal. Chem.*, 2011, **83**, 1193.
166 C.-L. Liu, H.-T. Wu, Y.-H. Hsiao, C.-W. Lai, C.-W. Shih, Y.-K. Peng, K.-C. Tang, H.-W. Chang, Y.-C. Chien, J.-K. Hsiao, J.-T. Cheng and P.-T. Chou, *Angew. Chem., Int. Ed.*, 2011, **50**, 7056.
167 C. Shao, B. Yuan, H. Wang, Q. Zhou, Y. Li, Y. Guan and Z. Deng, *J. Mater. Chem.*, 2011, **21**, 2863.
168 S. D. Haveli, P. Walter, G. Patriarche, J. Ayache, J. Castaing, E. E. Van, G. Tsoucaris, P.-A. Wang and H. B. Kagan, *Nano Lett.*, 2012, **12**, 6212.
169 M. Li, D.-P. Yang, X. Wang, J. Lu and D. Cui, *Nanoscale Res. Lett.*, 2013, **8**, 182.
170 Y. Liu, K. Ai, X. Cheng, L. Huo and L. Lu, *Adv. Funct. Mater.*, 2010, **20**, 951.
171 J.-M. Liu, M.-L. Cui, X.-X. Wang, L.-P. Lin, L. Jiao, Z.-Y. Zheng, L.-H. Zhang and S.-L. Jiang, *Sens. Actuators, B*, 2013, **188**, 53–58.
172 L. Hu, Y. Yuan, L. Zhang, J. Zhao, S. Majeed and G. Xu, *Anal. Chim. Acta*, 2013, **762**, 83.
173 M. A. H. Muhammed and T. Pradeep, in *Advanced Fluorescence Reporters in Chemistry and Biology II*, ed. A. P. Demchenko, Springer, Berlin Heidelberg, 2010, vol. 9, p. 333.
174 J.-M. Liu, J.-T. Chen and X.-P. Yan, *Anal. Chem.*, 2013, **85**, 3238.
175 G. Guan, S.-Y. Zhang, Y. Cai, S. Liu, M. S. Bharathi, M. Low, Y. Yu, J. Xie, Y. Zheng, Y.-W. Zhang and M.-Y. Han, *Chem. Commun.*, 2014, **50**, 5703.
176 G. Xavier Le, D. Nicole and S. Marc, *Nanotechnology*, 2011, **22**, 275103.
177 A. Baksi and T. Pradeep, *Nanoscale*, 2013, **5**, 12245.
178 A. Baksi, T. Pradeep, B. Yoon, C. Yannouleas and U. Landman, *ChemPhysChem*, 2013, **14**, 1272.